Introduction to Geophysical Fluid Dynamics

– *Computer Exercises* –

The 1st KAGI 21 INTERNATIONAL SUMMER SCHOOL

at the Institut Teknologi Bandung, Indonesia, July 11-26, 2004

KAGI 21

Kyoto University Active Geosphere Investigation
for the 21st Century COE Program

Conditions

Our software is all copyrighted by the authors of the book "Introduction to Geophysical Fluid Dynamics – Computer Exercises –" and KAGI21. We developed the software using MATLAB$^{®}$.©1984-2002 The MathWorks, Inc. Our limited rights to our software are governed by a certain license agreement between The MathWorks, Inc. and us.

For fast calculation and user convenience in exercises, approximate expressions and/or simplified simulation system are used in our software. We make no warranty that our software reproduce fully accurate physical process under arbitrary initial parameters. We accept no responsibility when you publish manuscripts, papers, or reports based on numerical results of our software.

Our software is furnished "as is". We make no warranty, express or implied, that our software is free of error, or is consistent with any particular standard of merchantability, or that it will meet your requirements for any particular application. We accept no responsibility for any mathematical or technical limitations of the procedures and functions which make up our software. Our software should not be relied on for solving a problem whose incorrect solution could result in injury to a person or loss of property. Neither KAGI21, nor Kyoto University, nor the authors of the book "Introduction to Geophysical Fluid Dynamics – Computer Exercises –", nor the contributors shall in any event be liable for any damages, whether direct or indirect, special or general, consequential or incidental, arising from use of our software. Your use of our software is entirely at your own risk.

Contents

Chapter 1

Introduction

1.1 KAGI 21 Software Library

As one of the education and research projects of the Kyoto University Active Geosphere Investigation (KAGI 21), which is one of the 21st Century Centers of Excellence (COE) program focusing on a new interdisciplinary approach to the Earth sciences from Asia and Oceania, we have collected computer programs designed for numerical modeling and simulations to organize them as a education material for students and young scientists who wish to study basic nonlinear and stochastic processes involved in various phenomena in the field of Earth sciences.

As the first trial of the project, we have integrated tutorial computer programs prepared by Prof.Shigeo Yoden and Prof.Satoshi Sakai into a common format with a user-friendly interface that facilitates execution of the programs on different kinds of computers. Since computation results from these programs need to be visualized in various forms of graphical outputs, we have made use of the MATLAB® graphics by converting the original programs written in FORTRAN (77 and 90) into the MATLAB programming language. The MATLAB source programs are further converted into application programs by the MATLAB compiler so that they can be distributed and executed on computers without the MATLAB license.

We hope the KAGI 21 Software Library will help students learn basic physical processes described by a set of differential equations and apply their experience with these computer programs to their study and reserach on various complex phenomena in Earth Sciences.

1.2 How to use a Graphical User Interface of MATLAB programs

This chapter gives a tutorial on GUI for the MATLAB programs contained in the "KAGI21 Summer School CD-ROM". These application programs enable us to carry out all exercises at the end of each chapter. We can easily access each application program through the main GUI, "*GFD Menu*" (Figure 1.1), provided by the program "`gfdmenu.exe`" in the CD-ROM and carry out various numerical experiments through the GUI.

Figure 1.2 shows an example of the GUI: all application programs use the common style of GUI as shown in Figure 1.2.

1. To select initial parameters

In parameter boxes provided in the application window, several sets of parameters have already been specified. Since these default parameters are prepared for running typical exercises, select one of these parameters by clicking the parameter box as your first trial.
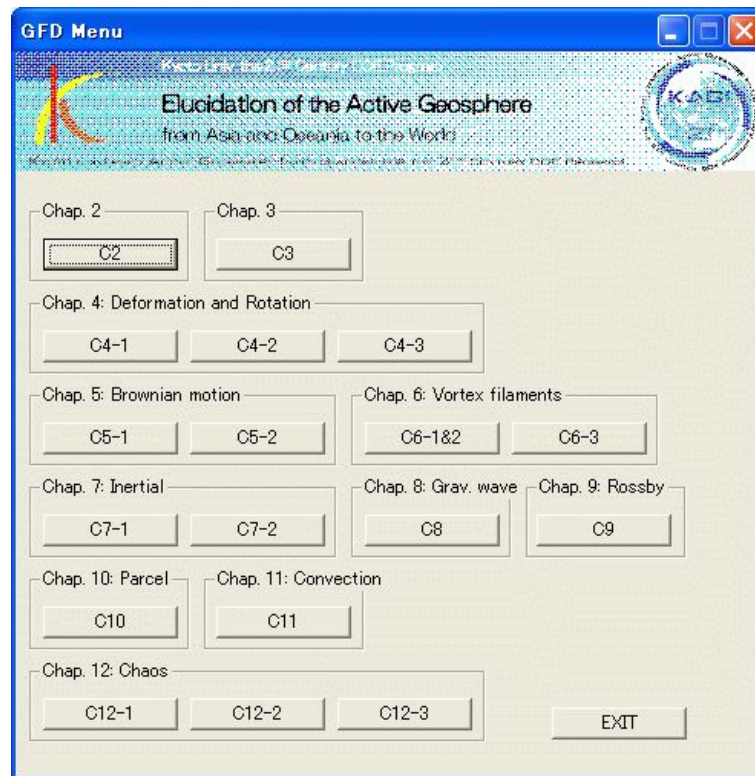
Figure 1.1: Main GUI of KAGI 21 Software, "*GFD Menu*".
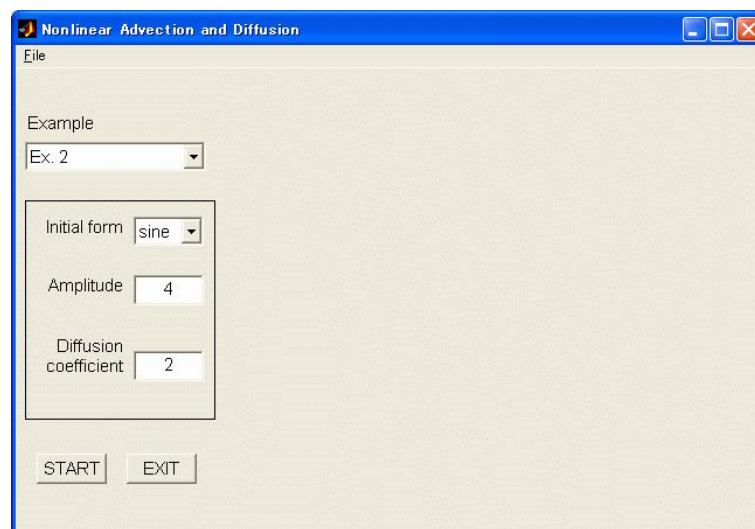
Figure 1.2: Example of the GUI.
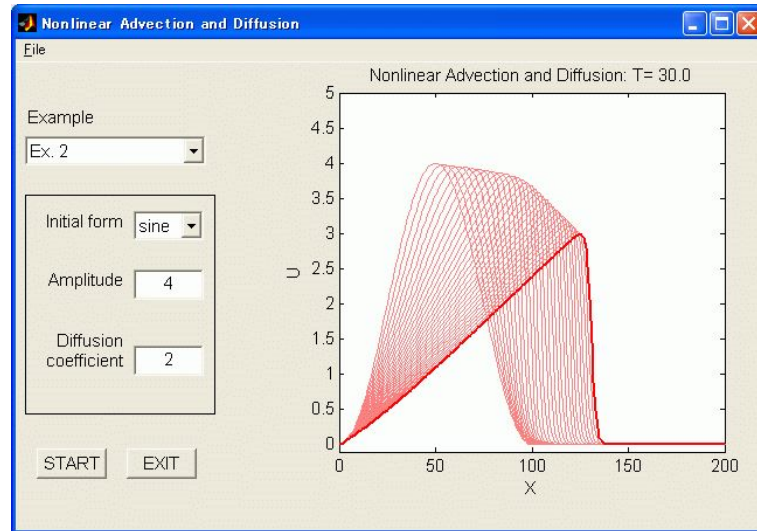
Figure 1.3: Example of an output of a numerical experiment.

2. To carry out a numerical experiment

In the application window, a button labeled "START" is provided. By clicking the "START" button, both temporal and spatial evolutions of physical values will be displayed in the graphic window until the end of the calculation.

3. To change parameters and perform other runs

After selecting the parameter box, key in arbitrary parameters for other experiments.

Since all input parameters have physical meanings, a different set of parameters results in a physically different result. Variations displayed in the graphic window are the result of the numerical simulation based on the basic equations described in each chapter. Therefore, all variations in the each experiment can be explained physical processes. By selecting various parameters and observing the changes in the numerical experiments, we can obtain a deep understanding of physical processes implemented by the basic equations. Try to perform your own numerical experiments by selecting different parameters in accordance with the description given in each chapter.

Chapter 2

Linear Advection and Diffusion

In this chapter, we analytically solve the one-dimensional linear advection-diffusion equation and see its time evolution. The observation of such time evolution will facilitate our understanding of the physical nature of advection and diffusion.

2.1 Theoretical background

We assume a one-dimensional linear advection-diffusion equation,

$$\frac{\partial u}{\partial t} + c\frac{\partial u}{\partial x} = \kappa\frac{\partial^2 u}{\partial x^2}, \tag{2.1}$$

where $u = u(x,t)$ is a function of the (one-dimensional) spatial coordinate x and time t. The constants c and κ are the advection velocity and the diffusion coefficient, respectively. The equation has the form common to all physical quantities. For example, when u is a momentum, the diffusion coefficient κ corresponds to the kinematic viscosity.

Based on whether c and/or κ are zero or not, the situation is classified into three conditions: linear advection ($c \neq 0, \kappa = 0$), diffusion ($c = 0, \kappa \neq 0$), and advection-diffusion ($c \neq 0, \kappa \neq 0$).

2.1.1 Linear advection

We set $\kappa = 0$ in the equation (2.1),

$$\frac{\partial u}{\partial t} + c\frac{\partial u}{\partial x} = 0. \tag{2.2}$$

We can find the analytical solution of this equation for the initial condition $u(x,0) = \varphi(x)$.

$$u(x,t) = \varphi(x - ct). \tag{2.3}$$

When $c > 0$, this solution represents the motion in the positive direction of the x axis with constant velocity c without changing the shape.

2.1.2 Diffusion

When we set $c = 0$ in (2.1), we obtain a diffusion equation,

$$\frac{\partial u}{\partial t} = \kappa\frac{\partial^2 u}{\partial x^2}. \tag{2.4}$$

Following Yoshida (1976) and Oikawa (1997), we solve this equation with the initial condition of $u(x,0) = \varphi(x)$ ($-\infty < x < \infty$).

First, we obtain a particular solution using the method of separation of variables. By separating the variables as $u(x, t) = X(x)T(t)$, we can rewrite (2.4) as

$$X(x)T'(t) = \kappa X''(x)T(t),$$
$$\frac{T'(t)}{\kappa T(t)} = \frac{X''(x)}{X(x)}. \tag{2.5}$$

Since the left-hand-side of this equation depends only on t and the right-hand-side does only on x, each of them has neet to be a constant. When we set this constant to $-\lambda^2$,

$$\begin{cases} T'(t) + \kappa\lambda^2 T(t) = 0, \\ X''(x) + \lambda^2 X(x) = 0. \end{cases} \tag{2.6}$$

Therefore,

$$T(t) = e^{-\kappa\lambda^2 t}. \tag{2.7}$$

If $X''(x) + \lambda^2 X(x) = 0$ has a solution not identical to zero, $u(x, t) = e^{-\kappa\lambda^2 t}X(x)$ is the nontrivial particular solution. As there is no boundary condition $(-\infty < x, \infty)$, however, it is impossible to get the eigenvalues for this equation. Thus, the eigenfunction can only be expressed as

$$X(x) = A(\lambda)\cos\lambda x + B(\lambda)\sin\lambda x. \tag{2.8}$$

Note that $A(\lambda)$ and $B(\lambda)$ are functions of λ. Therefore,

$$u(x, t) = e^{-\kappa\lambda^2 t}(A(\lambda)\cos\lambda x + B(\lambda)\sin\lambda x). \tag{2.9}$$

Because there is no eigenvalue, the sum of the particular solutions constitutes an integral. When $\lambda > 0$,

$$u(x, t) = \int_0^\infty e^{-\kappa\lambda^2 t}(A(\lambda)\cos\lambda x + B(\lambda)\sin\lambda x)d\lambda. \tag{2.10}$$

for $t \geq 0$.

Applying the Fourier's theorem to the initial condition φx, we obtain

$$\varphi(x) = \frac{1}{\pi}\int_0^\infty d\lambda \int_{-\infty}^\infty \varphi(\xi)\cos\lambda(x - \xi)d\xi,$$
$$= \frac{1}{\pi}\int_0^\infty \left\{\cos\lambda x \int_{-\infty}^\infty \varphi(\xi)\cos\lambda\xi d\xi + \sin\lambda x \int_{-\infty}^\infty \varphi(\xi)\sin\lambda\xi d\xi\right\} d\lambda. \tag{2.11}$$

When $t = 0$, (2.10) becomes

$$u(x, 0) = \int_0^\infty \{A(\lambda)\cos\lambda x + B(\lambda)\sin\lambda x\}d\lambda. \tag{2.12}$$

Since $u(x, 0) = \varphi(x)$, comparison between (2.11) and (2.12) yields

$$\begin{cases} A(\lambda) = \dfrac{1}{\pi}\displaystyle\int_{-\infty}^\infty \varphi(\xi)\cos\lambda\xi d\xi, \\ B(\lambda) = \dfrac{1}{\pi}\displaystyle\int_{-\infty}^\infty \varphi(\xi)\sin\lambda\xi d\xi. \end{cases} \tag{2.13}$$

Substituting these equations into (2.10), we obtain the following solution.

$$u(x, t) = \frac{1}{\pi}\int_{-\infty}^\infty \varphi(\xi)\left\{\int_0^\infty e^{-\kappa\lambda^2 t}\cos\lambda(x - \xi)d\lambda\right\} d\xi. \tag{2.14}$$

Since this equation includes two integrals and is thus complicated, we use

$$\int_0^\infty e^{-\alpha\lambda^2} \cos\beta\lambda\, d\lambda = \sqrt{\frac{\pi}{4\alpha}}\, e^{-\frac{\beta^2}{4\alpha}}, \qquad (\alpha > 0). \tag{2.15}$$

to simplify it, and finally obtain

$$u(x,t) = \int_{-\infty}^\infty \frac{\varphi(\xi)}{\sqrt{4\pi\kappa t}} \exp\left[-\frac{(x-\xi)^2}{4\kappa t}\right] d\xi, \qquad (t > 0). \tag{2.16}$$

As we can recognize by the form of (2.16), this is a Gaussian function, and $u = u(x,t)$ approaches zero as $t \to \infty$. Therefore, an arbitrary distribution given as the initial condition tends to become spatially uniform as time evolves. The rate of diffusion depends on the diffusion coefficient $\kappa(> 0)$.

2.1.3 Advection and diffusion

In this subsection, we discuss the case that $c \neq 0$ and $\kappa \neq 0$. We write down the equation (2.1) again.

$$\frac{\partial u}{\partial t} + c\frac{\partial u}{\partial x} = \kappa\frac{\partial^2 u}{\partial x}. \tag{2.17}$$

First, we apply the following coordinate transformation to obtain the analytical solution,

$$\begin{cases} X = x - ct, \\ T = t, \end{cases} \tag{2.18}$$

where (X, T) is a coodinate system moving at a constant velocity c. When $U(X,T) = u(x,t)$,

$$\frac{\partial u}{\partial t} = \frac{\partial U}{\partial X}\frac{\partial X}{\partial t} + \frac{\partial U}{\partial T}\frac{\partial T}{\partial t} = -c\frac{\partial U}{\partial X} + \frac{\partial U}{\partial T}, \tag{2.19}$$

$$\frac{\partial u}{\partial x} = \frac{\partial U}{\partial X}\frac{\partial X}{\partial x} + \frac{\partial U}{\partial T}\frac{\partial T}{\partial x} = \frac{\partial U}{\partial X}. \tag{2.20}$$

Similarly,

$$\frac{\partial^2 u}{\partial x^2} = \frac{\partial^2 U}{\partial X^2}. \tag{2.21}$$

When these are substituted into (2.17), we obtain a diffusion equation,

$$\frac{\partial U}{\partial T} = \kappa\frac{\partial^2 U}{\partial X^2}, \tag{2.22}$$

which means that an advection-diffusion equation (2.17) is equivalent to a diffusion equation when it is formulated under an appropriate moving coordinate system. As the solution of the diffusion equation is given by (2.16), $U(X,T)$ is proved to be

$$U(X,T) = \int_{-\infty}^\infty \frac{\varphi(\xi)}{\sqrt{4\pi\kappa T}} \exp\left[-\frac{(X-\xi)^2}{4\kappa T}\right] d\xi. \tag{2.23}$$

Thus, by inversely transforming the coordinate system to (x,t), we obtain the solution of (2.17) as

$$u(x,t) = \int_{-\infty}^\infty \frac{\varphi(\xi)}{\sqrt{4\pi\kappa t}} \exp\left[-\frac{(x-ct-\xi)^2}{4\kappa t}\right] d\xi. \tag{2.24}$$

When $c > 0$, this solution represents a move in the positive direction of the x axis with constant velocity c and with diffusion, which is consistent to the fact that the governing equation is a diffusion equation under an appropriate moving coordinate system.
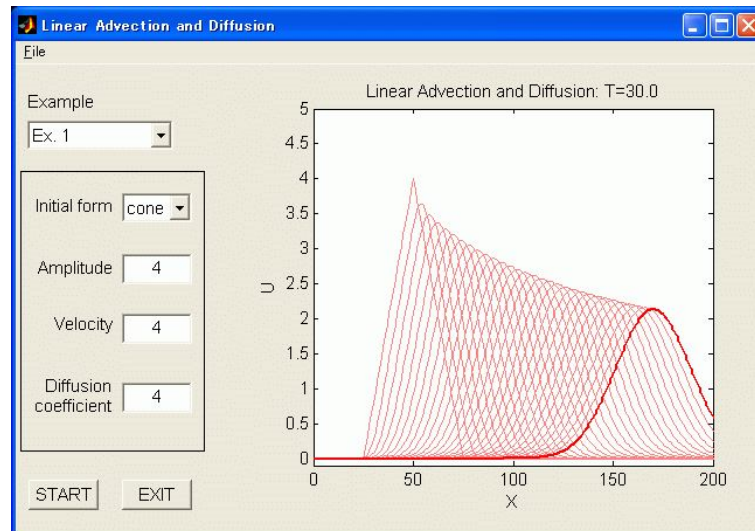
Figure 2.1: Result of Example 1.

2.2   Exercises

As the standard experiments, the following parameters have already specified in the program "C2" in GFD Menu. Note that "*velocity*" and "*diffusion coefficient*" shown in the GUI represents c and κ, respectively.

Example 1. advective diffusion $c = 4$, $\kappa = 4$.

Example 2. advection $c = 4$, $\kappa = 0$.

Example 3. diffusion $c = 0$, $\kappa = 4$.

The number shown as "*amplitude*" represents the hight of the initial function which can be input at will. We can also choose the shape of the initial function from among sinusoidal, step and cone-shaped functions. When doing experiments, keep the followings in mind:

in Example 1: What can be understood by looking at the simultaneous evolution of advection and diffusion? Is there any phenomena corresponding to advection-diffusion in the real world?

in Example 2: What can be understood by changing the advection velocity, initial condition, and its maximum value?

in Example 3: Consider what kind of characteristics diffusion has by changing the diffusion co-efficient and initial condition. What causes those characteristics?

References

Masayuki Oikawa, 1997 :Basic mathematics for scientists 4, Partial differential equation, 254pp (in Japanese)

Kousaku Yoshida, 1976 :Numerical analysis and its surroundings 5, An introduction to mathematical methods in physics, 198pp (in Japanese)

Chapter 3

Nonlinear Advection and Diffusion

In this chapter we solve the 1-D nonlinear advection-diffusion problem by numerical method. In contrast to the linear equation described in the previous chapter, here we discuss the nonlinear advection. Especially, we solve the *Burgers equation*.

3.1 Theoretical Background

3.1.1 Nonlinear Advection Equation

Assuming the finite-amplitude wave in the fluid which propagate only in direction (1-D x-t plane), the equation of motion is

$$\frac{Du}{Dt} = 0, \tag{3.1}$$

where viscosity, heat conductance and pressure gradient are ignored. In the Eulerian frame for x-t plane, the Lagrange differential of (3.1) can be rewritten as

$$\frac{\partial u}{\partial t} + u\frac{\partial u}{\partial x} = 0. \tag{3.2}$$

For the solution of (3.2), u is constant on the curve $Dx/Dt = u$. Each point of the wave form propagates at different speed, i.e., the speed is fast (slow) where u is high (low). Where the gradient $\partial u/\partial x$ is positive, it decreases with time to approach zero. Meanwhile, where the gradient is negative, it once diverges to -∞. After the appearance of -∞, (3.2) can no longer describe the phenomenon correctly, which is caused by the omission of the viscosity.

3.1.2 Burgers Equation

Adding the diffusive term in the right side of (3.2) to incorporate for represents the effect of viscosity, the equation is written as,

$$\frac{\partial u}{\partial t} + u\frac{\partial u}{\partial x} = \nu\frac{\partial^2 u}{\partial x^2}. \tag{3.3}$$

This is called *Burgers Equation*, which we can solve analytically (Tatsumi, 1982). Using the Cole-Hopf transformation (Hope,1950; Cole,1951),

$$u = -2\nu\frac{\partial}{\partial x}\log\theta, \tag{3.4}$$

$$\theta(x,t) = \exp\left[-\frac{1}{2\nu}\int^x u(x',t)dx'\right], \tag{3.5}$$

the diffusion equation for $\theta(x,t)$ is

$$\frac{\partial \theta}{\partial t} = \nu \frac{\partial^2 \theta}{\partial x^2}. \tag{3.6}$$

The general solution of (3.6) is

$$\theta(x,t) = \frac{1}{\sqrt{4\pi\nu t}} \int_{-\infty}^{\infty} \theta(x',0) \exp\left[-\frac{(x-x')^2}{4\nu t}\right] dx', \tag{3.7}$$

where $\theta(x,0)$ is the initial condition (see also 2.1.2). Consequently the general solution of the Burgers equation is as follow,

$$u = -2\nu \frac{\partial}{\partial x} \log\left(\frac{1}{\sqrt{4\pi\nu t}} \int_{-\infty}^{\infty} \exp\left[-\frac{1}{2\nu}\left\{\frac{(x-x')^2}{2t} + U(x')\right\}\right] dx'\right), \tag{3.8}$$

$$\text{where} U(x) = \int^{x} u(x',0)dx'. \tag{3.9}$$

3.2 Exercises

3.2.1 Nonlinear Advection Equation

We solve the equation (3.2) with no viscosity ($\nu = 0$) by the numerical method, and study the time development for some initial conditions. Observe the wave form be gradually distorted and finally break.

Example 1

	sine	4	0
	Initial function	Amplitude	Diffusion

Since the wave breaking is caused by the limitation of the numerical method, there is no meaning of the solution. Change the amplitude, and observe the result that the starting time of the wave breaking depends on the advection speed. We can also examine the distorting processes by changing the initial wave forms (sine, cone, and step functions).

To study nonlinear advection and diffusion numerically, carry out the program "C3" in GFD Menu.

3.2.2 Burgers Equation

We solve the Burgers equation (3.3) with viscosity ($\nu \neq 0$).

Example 2

	sine	4	2
	Initial function	Amplitude	Diffusion

When the local diffusion is large, there is an appropriate range of parameters in which the wave keeps its standing form. Find out the range by changing the ratio `amplitude/diffusion`.

3.3 Appendix

We use the 4th order *Runge Kutta Gill Method* for integration with respect to time, and also use the *Central Difference* for space differences in the numerical experiments. These numerical schemes are unstable for $\nu > 7$ (Nishizawa, 1999). Here the stability of the difference method is investigated according to Horinouchi (1996).
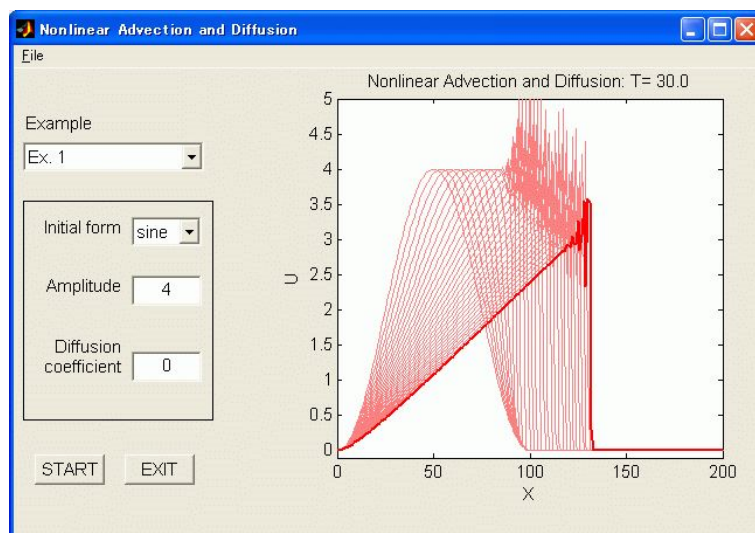
Figure 3.1: Result of Example 1.

Reference

Cole, J., 1951: On a quasi-linear parabolic equation occuring inaerodynamics. *Q.Appl.Math.*, **9**, 225-236.

Hopf, E., 1950: The partial differential equation $u_t + uu_x = u_{xx}$. *Common.Pure Appl.Math.*, **3**, 201-230.

Horinouchi T., 1996: Practice D5 & Programs (in Japanese).

Nishizawa., S., 1999: Note for numerical calculation of Burgers equation (in Japanese).

Tatsumi, T., 1982: Fluid Dynamics, *Baifukan*, 453pp (in Japanese).

Chapter 4

Deformation and Rotation − Lagrange Recognition

In this chapter, we study the advection of the fluid parcels with time in the steady two-dimensional flow. The process of deformation of fluid parcel is decided by *deformation rate tensor*.

4.1 Theoretical Background

4.1.1 Deformation of fluid

In case of time-invariant steady flow with letting $\mathbf{u} = (u_1, u_2, u_3)$ be the velocity of the fluid, the equation of motion for fluid parcel is given by

$$\frac{d\mathbf{x}}{dt} = \mathbf{u}(\mathbf{x}). \tag{4.1}$$

The motion of fluid parcel can be traced by integrating (4.1) in time. Assuming that $\mathbf{x}(t)$ is the trajectory of the fluid parcel, we consider the time development of the trajectory of the parcel which slightly deviated from $\mathbf{x}(t)$ (Mizuta, 1999; p.5-8). Letting $\mathbf{y}(t)$ be this small displacement, we obtain its development with time as

$$\begin{aligned}\frac{d}{dt}(\mathbf{x}(t) + \mathbf{y}(t)) &= \mathbf{u}(\mathbf{x}(t) + \mathbf{y}(t), t), \\ &= \mathbf{u}(\mathbf{x}(t), t) + (\nabla \mathbf{u})^T \mathbf{y}(t) + O(\mathbf{y}^2). \end{aligned} \tag{4.2}$$

Subtracting (4.1) from this, ignoring the $O(\mathbf{y}^2)$-term and linearizing locally, we obtain

$$\frac{d\mathbf{y}(t)}{dt} = J(\mathbf{x}(t))\mathbf{y}(t). \tag{4.3}$$

Here J is the Jacobian of $\mathbf{u}$ at $\mathbf{x}(t)$ given by

$$J = (\nabla \mathbf{u})^T = \begin{pmatrix} \frac{\partial u_1}{\partial x_1} & \frac{\partial u_1}{\partial x_2} & \frac{\partial u_1}{\partial x_3} \\ \frac{\partial u_2}{\partial x_1} & \frac{\partial u_2}{\partial x_2} & \frac{\partial u_2}{\partial x_3} \\ \frac{\partial u_3}{\partial x_1} & \frac{\partial u_3}{\partial x_2} & \frac{\partial u_3}{\partial x_3} \end{pmatrix}, \tag{4.4}$$

which is called *deformation rate tensor*. By investigating the characteristics of J, we can understand the deformation of the continuum.

4.1.2   Deformation of two-dimensional fluid – analysis with eigenvalue –

The deformation in the two-dimentional fluid can investigate by categorizing J. Generally, 2×2-matrix is categorized as the following three types in attempting diagonalization.

$$\mathbf{A}: \begin{pmatrix} \lambda & 0 \\ 0 & \mu \end{pmatrix}, \qquad \mathbf{B}: \begin{pmatrix} a & -b \\ b & a \end{pmatrix}, \qquad \mathbf{C}: \begin{pmatrix} \lambda & 0 \\ 1 & \lambda \end{pmatrix}. \tag{4.5}$$

Based on (4.5), the flow field can be classified as follows.

$\quad$ **A**: In a case that J can be diagonalized and has real eigenvalues,

$$\frac{d}{dt} \begin{pmatrix} y_1 \\ y_2 \end{pmatrix} = \begin{pmatrix} \lambda & 0 \\ 0 & \mu \end{pmatrix} \begin{pmatrix} y_1 \\ y_2 \end{pmatrix}, \tag{4.6}$$

$$y_1 = y_1(t_0)e^{\lambda t}, \qquad y_2 = y_2(t_0)e^{\mu t}. \tag{4.7}$$

- **A1**: when $\lambda = \mu$, the point $\mathbf{x}$ is a *focus*.

- **A2**: when λ and μ have the same sign, $\mathbf{x}$ is a *node*.

- **A3**: when λ and μ have the different sign, $\mathbf{x}$ is a *saddle*.

$\quad$ **B**: In a case that the eigenvalues are complex conjugates,

$$\frac{d}{dt} \begin{pmatrix} y_1 \\ y_2 \end{pmatrix} = \begin{pmatrix} a & -b \\ b & a \end{pmatrix} \begin{pmatrix} y_1 \\ y_2 \end{pmatrix}, \tag{4.8}$$

$$(y_1, y_2)^T = (y_1(t_0), y_2(t_0))^T e^{(a+ib)t}. \tag{4.9}$$

- **B1**: when $a \neq 0$, $\mathbf{x}$ is a *spiral*.

- **B2**: when $a = 0$, $\mathbf{x}$ is a *center*.

$\quad$ **C**: In a case that J can not be diagonalized,

$$\frac{d}{dt} \begin{pmatrix} y_1 \\ y_2 \end{pmatrix} = \begin{pmatrix} \lambda & 0 \\ 1 & \lambda \end{pmatrix} \begin{pmatrix} y_1 \\ y_2 \end{pmatrix}. \tag{4.10}$$

- **C1**: when $\lambda \neq 0$, $\mathbf{x}$ is an *improper node*.

- **C2**: when $\lambda = 0$, $\mathbf{x}$ is a *simple shear*.

Based on the discriminant of the eigenvalue equation $\Delta = (\text{tr}J)^2 - 4\det J$, we can classify the flow field, i.e., **A**, **B** and **C** correspond to the cases that $\Delta \geq 0$, $\Delta < 0$ and $\Delta = 0$. Figure 4.1 shows the relationship on the two-dimensional plain with $\text{tr}J$ and $\det J$ axes. Since $\text{tr}J = \sum \partial u_i / \partial x_i$, the flow is non-divergent over y-axis, while the flow is divergent and convergent on the right and left side, respectively. The parabola through the origin indicates the curve where $\Delta = 0$. Over this line $\mathbf{x}$ is a focus (**A**) or an improper node (**C**), and at the origin $\mathbf{x}$ is a simple shear (**C**). Above this line, $\Delta < 0$ where $\mathbf{x}$ is a spiral or a center. On the other hand, since the discriminant $\Delta > 0$ below this line, in this domain $\mathbf{x}$ is a node and a saddle above ($\det J > 0$) and below x-axis ($\det J < 0$), respectively.
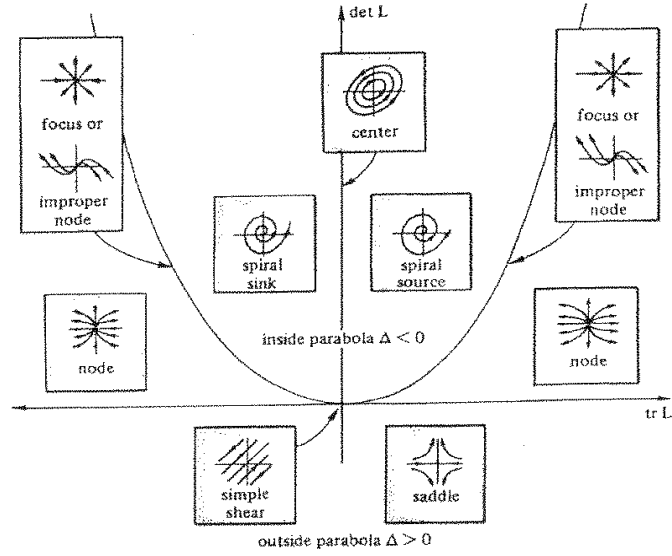
Figure 4.1: Classification of flow by the deformation rate tensor. After Ottino (1989; Fig. E2.5.2, p.27).

4.1.3 Strain rate tensor and tensor for the rotation

Based on the text of Tatsumi (1995; p.43-48), we continue considering the deformation rate tensor.

As in previous subsection, the effect of deformation by fluid motion is described by the deformation rate tensor $\nabla \mathbf{u} = \partial u_i / \partial x_j$. Dividing this into symmetric and asymmetric components, we obtain

$$\frac{\partial u_i}{\partial x_j} = e_{ij} + \omega_{ij}, \tag{4.11}$$

$$e_{ij} = \frac{1}{2} \left(\frac{\partial u_i}{\partial x_j} + \frac{\partial u_j}{\partial x_i} \right), \tag{4.12}$$

$$\omega_{ij} = \frac{1}{2} \left(\frac{\partial u_i}{\partial x_j} - \frac{\partial u_j}{\partial x_i} \right), \tag{4.13}$$

where e_{ij} represents local deformation, and is called *strain rate tensor*. On the other hand, ω_{ij} represents rotating rigid motion, and is called *rotation displacement*.

The diagonal component of strain rate tensor $e_{ii} = \partial u_i / \partial x_i$ $(i = 1, 2, 3)$ represents the velocity of elongation-contraction along x_i axis. In addition, sum of the diagonal components,

$$\sum_i e_{ii} = \sum_i \frac{\partial u_i}{\partial x_i} = div\mathbf{u}, \tag{4.14}$$

represents *volume dilatation rate*. This is the variation ratio of the volume by elongation or contraction. In case of two-dimensional motion, it represents the variation of the area by elongation or contraction. On the other hand, asymmetric component e_{ij} represents the velocity of the variation of the angle between x_i and x_j axis, which is called *shear strain rate*.

The asymmetric components of deformation rate tensor ω_{ij} can be written as with vector $\omega = (\omega_1, \omega_2, \omega_3)$ and Eddington sign ϵ_{ijk}

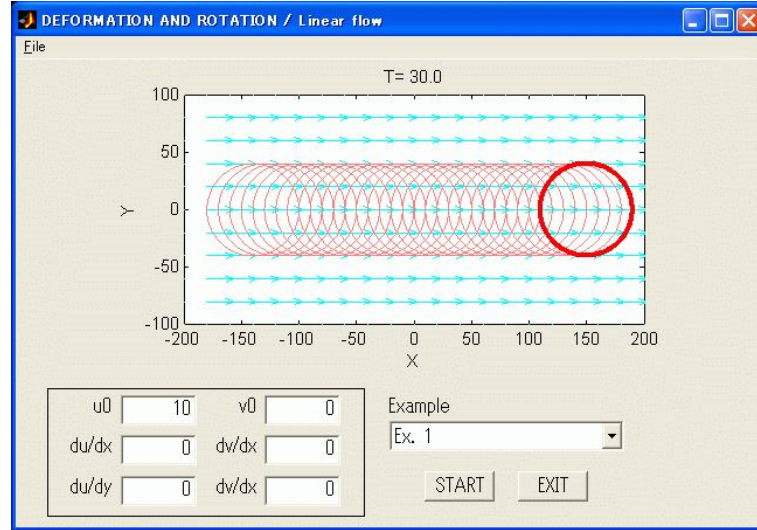$$\omega_{ij} = -\frac{1}{2} \sum_k \epsilon_{ijk} \omega_k, \qquad (i, j = 1, 2, 3) \tag{4.15}$$

Figure 4.2: Result of Example 1.

$$\omega_k = -\sum_i \sum_j \epsilon_{ijk}\omega_{ij}, \tag{4.16}$$

This equation can be rewritten as

$$\omega_k = -\frac{1}{2}\sum_i \sum_j \epsilon_{ijk}\left(\frac{\partial u_i}{\partial x_j} - \frac{\partial u_j}{\partial x_i}\right), \tag{4.17}$$

or in the vector form,

$$\omega = rot\mathbf{u}. \tag{4.18}$$

ω is the rotational component of the velocity $\mathbf{u}$ and is called *vorticity*. Let θ be the rotation angle, and (4.18) becomes

$$\omega = 2\dot{\theta}. \tag{4.19}$$

Vorticity ω is twice as large as the angular velocity of the displacement vector $\mathbf{r}$ and each coodinate component of ω $(\omega_1, \omega_2, \omega_3)$ is twice as large as the angular velocity around each axis.

4.2   Exercises

Observe the deformation of the fluid parcel in linear or axisymmetric flow field using the program "C4-1" (for Examples 1 ∼ 5), "C4-2" (for Examples 6 and 7), and "C4-3" (for Examples 8 ∼ 10) in GFD Menu.

4.2.1   Linear flow

Consider the steady and linear flow field as

$$u(x,y) = u_0 + \frac{du}{dx}x + \frac{du}{dy}y, \qquad v(x,y) = v_0 + \frac{dv}{dx}x + \frac{dv}{dy}y, \tag{4.20}$$

where $u_0, \frac{du}{dx}, \frac{du}{dy}, v_0, \frac{dv}{dx}$ and $\frac{dv}{dy}$ are constant. Since the flow field is linear, the characteristics of the deformation of the fluid is uniform and is independent of the size of the fluid parcel. That is, (4.3) is satisfied rigidly.

Set each constant in the configuration window. When starting the program, the fluid parcels settled around the circle initially can be traced with time and the deformation of the fluid parcel can be observed.

Example 1. Homogeneous flow

$$
\begin{array}{cccccc}
10.0 & 0.0 & 0.0 & 0.0 & 0.0 & 0.0 \\
\texttt{u0} & \texttt{du/dx} & \texttt{du/dy} & \texttt{v0} & \texttt{dv/dx} & \texttt{dv/dy}
\end{array}
$$

In this case, all the components of deformation rate tensor are zero. There is neither the deformation or rotation of the fluid, and the area does not change because of non-divergent flow. The fluid parcel is advected along x-axis with constant speed u_0, conserving initial circular pattern.

Example 2. Divergent flow

$$
\begin{array}{cccccc}
0.0 & 0.05 & 0.0 & 0.0 & 0.0 & 0.05 \\
\texttt{u0} & \texttt{du/dx} & \texttt{du/dy} & \texttt{v0} & \texttt{dv/dx} & \texttt{dv/dy}
\end{array}
$$

Following the classification by eigenvalue in section 4.1.2, the origin in this case becomes a focus. Dividing deformation rate tensor into strain rate tensor and tensor for rotation, there is no rotation since the latter is zero. By the diagonal component of the strain rate tensor e_{ii}, elongation-contraction by `dudx` and `dvdy` occurs in x- and y-direction, respectively. Since $div\mathbf{u} \neq 0$, the area of the fluid parcel changes. If setting `dudx` and `dvdy` with the same sign and different value, the origin becomes a node.

Example 3. Deformation field

$$
\begin{array}{cccccc}
0.0 & 0.05 & 0.0 & 0.0 & 0.0 & \text{-}0.05 \\
\texttt{u0} & \texttt{du/dx} & \texttt{du/dy} & \texttt{v0} & \texttt{dv/dx} & \texttt{dv/dy}
\end{array}
$$

Following the classification by eigenvalue, the origin becomes a saddle. strain rate tensor and tensor for rotation are the same as **Example 2**, while the changing rate of the area is zero because of non-divergent flow. elongation-contraction occurs in the direction of x- and y-axis, conserving the area of the fluid parcel. In addition, changing the value of `dvdy`, observe saddles with divergence.

Example 4. Rotation displacement

$$
\begin{array}{cccccc}
0.0 & 0.05 & \text{-}0.15 & 0.0 & 0.15 & 0.05 \\
\texttt{u0} & \texttt{du/dx} & \texttt{du/dy} & \texttt{v0} & \texttt{dv/dx} & \texttt{dv/dy}
\end{array}
$$

Both strain rate tensor and tensor for rotation are non-zero, and the flow is divergent with rotation. If `dudx` and `dvdy` are zero, the flow is non-divergent and center-type. The initial circular pattern is converved.

Example 5. Simple shear

$$
\begin{array}{cccccc}
0.0 & 0.0 & 0.15 & 0.0 & 0.0 & 0.0 \\
\texttt{u0} & \texttt{du/dx} & \texttt{du/dy} & \texttt{v0} & \texttt{dv/dx} & \texttt{dv/dy}
\end{array}
$$

In case of simple shear, dividing the deformation rate tensor into strain rate tensor and tensor for rotation gives

$$
\nabla \mathbf{u} = \begin{pmatrix} 0 & \frac{1}{2}\frac{\partial u}{\partial y} \\ \frac{1}{2}\frac{\partial u}{\partial y} & 0 \end{pmatrix} + \begin{pmatrix} 0 & \frac{1}{2}\frac{\partial u}{\partial y} \\ -\frac{1}{2}\frac{\partial u}{\partial y} & 0 \end{pmatrix}. \tag{4.21}
$$

Non-diagonal component of strain rate tensor e_{ij} represents the velocity of the variation of the angle between x-axis and y-axis, and a shear strain occurs around the perpendicular of x-y plain (z-axis). On the other hand, non-diagonal component of the tensor for rotation ω_{ij}, from (4.20), represents that the fluid parcel rotate around the perpendicular of x-y plain with angular velocity $\frac{1}{2}\frac{\partial u}{\partial x}$. The area does not change because of non-divergent flow.

4.2.2   Rotating axi-symmetric flow

Consider the situation 'Rankine's connected vortex' where the flow is two-dimensional and unelastic and the vorticity distributes homogeneously in the circle (Tatsumi, 1982; p.188-199). Letting a and ω be the radius of the vortex domain and the (vertical component of) vorticity respectively, given that the flow field is axisymmetric, and assume the flow function as the function of only the radius r. In this case, velocity field have only tangental component $v_\theta(r)$ and is written, dependent of the radius r, as

$$v_\theta = \begin{cases} \frac{\omega r}{2} & (r \leq a), \\ \frac{\omega a^2}{2r} & (r > a). \end{cases} \tag{4.22}$$

Set ω and a at `omega` and `edge` in the configuration box, respectively. When starting the program, the fluid parcels settled initially in square can be traced with time and the deformation of the fluid parcel can be observed. In addition, the initial position (x, y) of the fluid parcel (square) can be set explicitly at `xoffst` and `yoffst`.

Example 6. Rigid-rotating vortex

0.15	200.0	50.0	0.0
ω	Edge	X offset	Y offset

In the vortex domain $(r < a)$, the velocity can be rewritten in Cartesian coordinates (x, y) as $\mathbf{u} = (-\frac{\omega r}{2}\sin\theta, \frac{\omega r}{2}\cos\theta) = (-\frac{\omega}{2}y, \frac{\omega}{2}x)$, where $r = (x^2 + y^2)^{1/2}$. Since $div\mathbf{u} = 0$, the flow is non-divergent (it is natural because we introduce the streamfunction, assuming two-dimensional unelastic flow). Following the classification by eigenvalue in section 4.1.2, since $\mathrm{tr}J = 0$, $\det J > 0$ and $\Delta < 0$, the origin in this case corresponds to the center. When dividing deformation rate tensor into strain rate tensor and tensor for rotation, all the components of strain rate tensor are zero and the non-diagonal components of ω_{ij} remain. There is no strain and the fluid percel do the rigid rotation around the perpendicular of x-y plain (z-axis) with constant angular velocity $\frac{\omega}{2}$.

Example 7. Out of the votex

0.15	50.0	50.0	0.0
ω	Edge	X offset	Y offset

Out of the vortex domain $(r > a)$, the velocity can be rewritten in Cartesian coordinates as $\mathbf{u} = (-\frac{\omega a^2}{2r}\sin\theta, \frac{\omega a^2}{2r}\cos\theta) = (-\frac{\omega a^2}{2r^2}y, \frac{\omega a^2}{2r^2}x)$. Since $\mathrm{tr}J = 0$, $\det J < 0$ and $\Delta > 0$, the flow corresponds to the saddle. Deformation rate tensor can be rewritten as

$$\nabla\mathbf{u} = \begin{pmatrix} \frac{\omega a^2}{r^4}xy & \frac{1}{2}\frac{\omega a^2}{r^4}(y^2 - x^2) \\ \frac{1}{2}\frac{\omega a^2}{r^4}(y^2 - x^2) & -\frac{\omega a^2}{r^4}xy \end{pmatrix} + \begin{pmatrix} 0 & 0 \\ 0 & 0 \end{pmatrix}. \tag{4.23}$$

Each term in strain rate tensor have values dependent of x and y. By the diagonal component e_{ii}, elongation-contraction occurs in the direction of x- and y-axis and the strain propotional to r^{-2} exists in x-y plain. By the component e_{ij}, the fluid rotates around z-axis with strain, while vorticity is zero except for z-axis because $\omega_{ij} = 0$. The area does not change because of non-divergent flow.

4.3   Application

In the preveous section, the deformation rate tensor had the constant value everywhere in the linear flow field. However, in the realistic flow, deformation rate tensor variate complicatedly in space and time. In this section, study the deformation of the fluid parcel, by using the two-dimensional
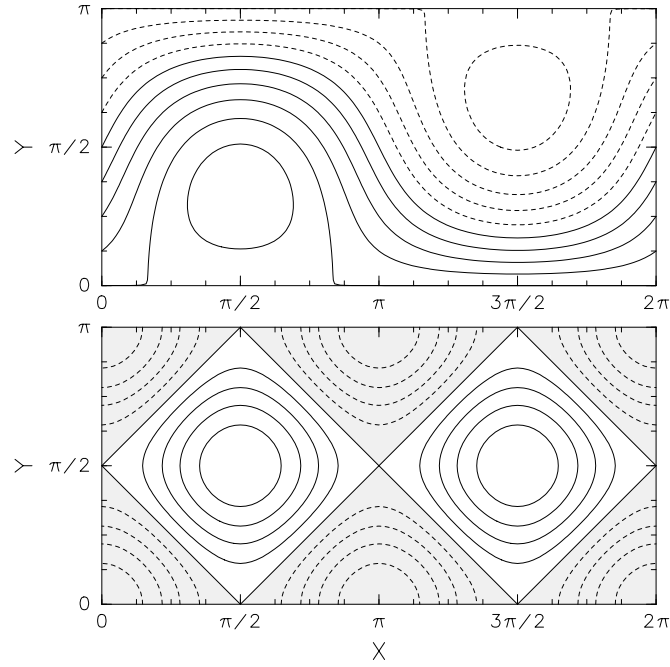
Figure 4.3: The distribution of two-dimensional non-divergent flow (upper panel) and det$J$ (lower panel) assuming Rossby wave. Hatched area indicates the domain for det$J < 0$.

non-divergent flow assuming Rossby wave taken up by Pierrehumbert (1991) in the paper on the caotic mixing.

Given the flow function $\psi(x, y) = A \sin k_1 x \sin l_1 y - u_0 y$ (upper panel of Figure 4.3). In this case, the velocity is

$$\begin{cases} u(x, y) = -\frac{\partial \psi}{\partial y} = -Al_1 \sin k_1 x \cos l_1 y + u_0, \\ v(x, y) = \frac{\partial \psi}{\partial x} = Ak_1 \cos k_1 x \sin l_1 y. \end{cases} \tag{4.24}$$

The value tr$J = 0$ because of non-divergent. In addition, det$J = -\cos^2 x \cos^2 y + \sin^2 x \sin^2 y$ and the flow is a center (det$J > 0$), a simple shear (det$J = 0$) or a saddle (det$J < 0$), dependent of the location (lower panel of Fig. 4.3). around the stagnation point over $y = 0, \pi$, the deformation of the fluid parcel is dominant, while in the positive and negative vortex the rotation is dominant.

Deformation rate tensor is

$$\nabla \mathbf{u} = \begin{pmatrix} -\cos x \cos y & 0 \\ 0 & \cos x \cos y \end{pmatrix} + \begin{pmatrix} 0 & \sin x \sin y \\ -\sin x \sin y & 0 \end{pmatrix}. \tag{4.25}$$

Both the diagonal component of strain rate tensor e_{ij} and the non-diagonal component of tensor for rotation ω_{ij} remain. An elongation and a contraction dependent of the location in the direction of x- and y-axis and a rotation with angular velocity $\sin x \sin y$ are observed.

Set the location of initial circle (X,Y), the radius of initial circle (r) and homogeneous background flow speed (u0) in the configuration box. When starting the program, the fluid parcels settled around the circle initially can be traced with time and the deformation of the fluid parcel can be observed.

Example 8. Winding jet

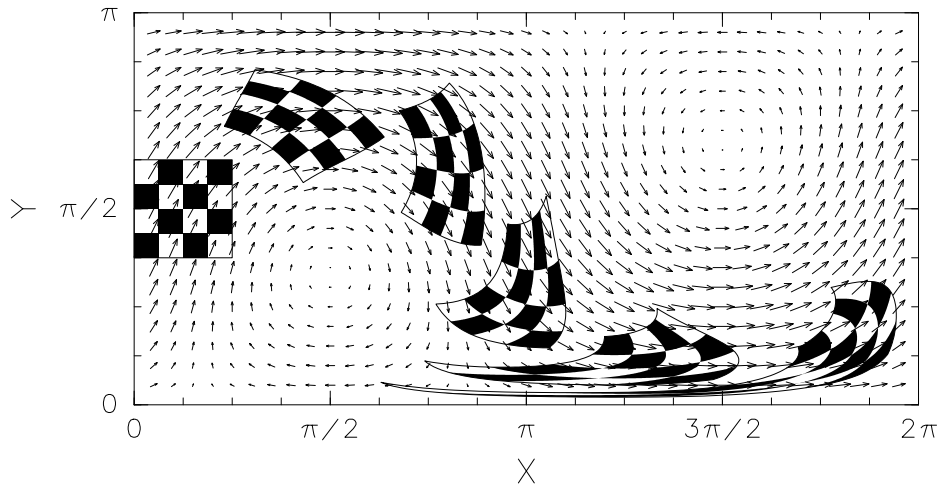| 0.9	1.6	0.1	0.5
X	Y	r	u0

Figure 4.4: The deformation of checker-flag pattern in two-dimensional non-divergent flow assuming Rossby wave.

Initially the fluid parcel is advected by jet flow with little strain. When the fluid parcel enter into the area where the deformation is dominant, it is heavily strained. Locate the initial circle around the center of the jet or in the vortex, and observe the difference dependent of the location.

Example 9. Vortex street

0.1	1.6	0.1	0.0
X	Y	r	u0

Make an experiment with setting the homogeneous background flow speed (u0) to zero, and compare with previous example.

Example 10. Checker-flag pattern

0.41	1.56	0.7854	0.5
X	Y	r	u0

Trace the fluid parcel having checker-flag pattern in the same two-dimensional non-divergent flow, and study the deformation (Figure 4.4). Modify the parameters and executes the program. By changing the condition, realize the relationship between the flow field and the deformation.

4.4   Appendix

Weiss (1990) classified the flow field by $\mathrm{tr}A^2$, where A is deformation rate tensor $\nabla\mathbf{u}$. In case that $\mathrm{tr}A^2 > 0$, the motion is hyperbolic and deformation of the fluid parcel is dominant. On the other hand, in case that $\mathrm{tr}A^2 < 0$ the motion is elliptic and rotation is dominant. Since

$$\mathrm{tr}A^2 = \frac{\partial^2\psi}{\partial x\partial y} - \frac{\partial^2\psi}{\partial x^2}\frac{\partial^2\psi}{\partial y^2} = \cos^2 x\cos^2 y - \sin^2 x\sin^2 y = -\det J, \qquad (4.26)$$

it just correspond with the classification at section 4.1.2. That is, hyperbolic and elliptic motion corresponds to the saddle and center, respectively.

References

Mizuta, R., 1999: Caotic mixing in quasi-periodic flow assuming the polar vortex in the strato-sphere. Master thesis, Kyoto University, 60 pp.

Ottino, J., 1989: *The kinematics of mixing: Stretching, chaos, and transport.* Cambridge University Press, 364 pp.

Pierrehumbert, R.T., 1991: Large-scale horizontal mixing in planetary atmospheres. *Phys. Fluids A*, **3**, 1250-1260.

Tatsumi, T., 1982: *Fluid dynamics.* Baifu-kan, 453 pp.

Tatsumi, T., 1995: *Continuum dynamics.* Iwanami, 334 pp.

Weiss, J., 1990: The dynamics of enstrophy transfer in two-dimensional hydrodynamics. *Physica D*, **48**, 273-294.

Chapter 5

Brownian Motion – Particle Diffusion by Stochastic Force

In this chapter, the motions of Lagrangian particles not in deterministic but in *stochastic* process is studied. This phenomenon is well known as *Brownian motion*. We will calculate the tracks of particles forced by random number sequence.

5.1 Theoretical Background

We summarize the discovery and following researches of Brownian motion according to Kobayashi [1983; section 2-8].

Robert Brown, who is a famous Scottish botanist for his discovery of the nucleus in the plant cell, first observed Brownian motion in 1827. He studied pollen grains suspended in a liquid with a microscope, and noticed a random oscillatory motion of the microparticles. He interpreted that the motion belonged to the biotic particles themselves. Similar phenomena were found later for inorganic microparticles, and charcoal microparticles in a solution of India ink. These oscillations were clarified nothing but thermal fluctuations of huge molecules by L. G. Gouy in France. He showed that the motion was more rapid for smaller particles, for smaller viscosity of suspending medium, and for higher temperature. The molecular kinetic theory of heat was introduced and developed to treat these fluctuations of Brownian particles by A. Einstein in 1905 and by M. von Smoluchowski in 1906.

5.2 Models

There are two basic concepts to describe the Brownian motion; *Langevin model* and *random displacement model*. In the former, a particle trajectory is defined by time integral of random variations of its Lagrangian velocity. In the latter, the trajectory is given by sum of random displacement vector.

Hereafter, we treat the Langevin model which is introduced by P. Langevin and used to analyze Brownian motion in 1908 [refer section 2.1 of *Rodean*, 1996]. Here we assume that the Brownian particles are controlled by absolutely random force with no external force. The particles are moved by the random force due to the collision with molecules of suspending medium, and drifted by the viscosity which is linearly related to the velocity (Rayleigh friction) for average. Brownian motion is expressed by using the following equation,

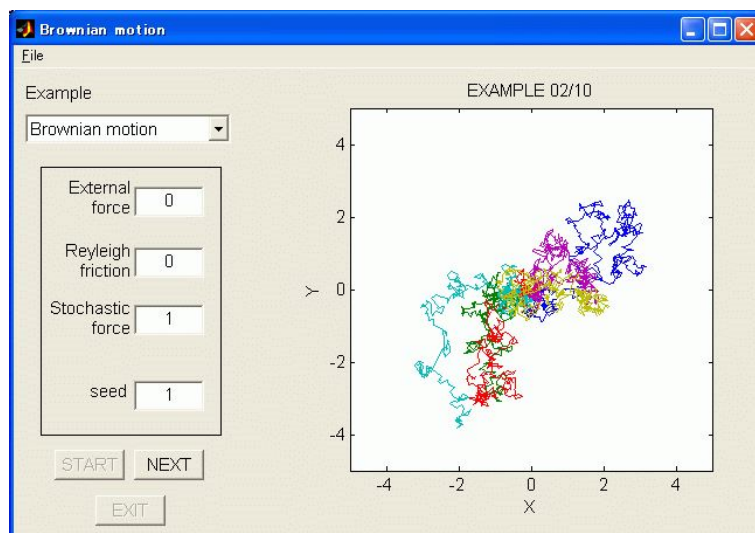$$\frac{d\mathbf{u}}{dt} = -a_1\mathbf{u} + b\xi(t), \tag{5.1}$$

Figure 5.1: Result of Example 1.

where t is time, $\mathbf{u}$ is velocity of a Brownian particle, a_1 is the coefficient of viscosity, and ξ denotes the random function. The second term of the right hand side shows the random acceleration of particles by collisions. Langevin deduced from (5.1) that;

- if $t \ll 1/a_1$, root mean square of particle displacement has linear relation to t^2,

- if $t \gg 1/a_1$, root mean square of particle displacement has linear relation to t.

These results are closely related with *diffusion process.*

In subsequent studies, acceleration terms by gravitational field and electric field were added to *Langevin equation* (5.1) as

$$\frac{d\mathbf{u}}{dt} = \mathbf{a_0} - a_1\mathbf{u} + b\xi(t). \tag{5.2}$$

A finite difference equation can be derived from (5.2),

$$\mathbf{u}_{i+1} = \mathbf{u}_i + (\mathbf{a_0} - a_1\mathbf{u}_i + b\xi_i)\Delta t, \tag{5.3}$$

where $\mathbf{u}_i$ denotes the velocity of a Brownian particle at time i, and a random function ξ_i is the i-th value of Gaussian deviates. The particle location, denoted $\mathbf{x}_i$, is defined by the following backward difference equation,

$$\mathbf{x}_{i+1} = \mathbf{x}_i + \mathbf{u}_{i+1}\Delta t. \tag{5.4}$$

In the next section, we solve these finite difference equations numerically.

5.3 Exercises

Example 1 Tracks of Brownian particles

Run the program "C5-1" to trace trajectories of Brownian particles. Click the START button in the application window, and display the time development of locations of 6 particles with 6 colors. Both parameters External force ($\mathbf{a_0}$) and Rayleigh friction (a_1) are set 0 for default, and begin this experiment with the basic condition that neither external field nor viscosity accelerates the particles.

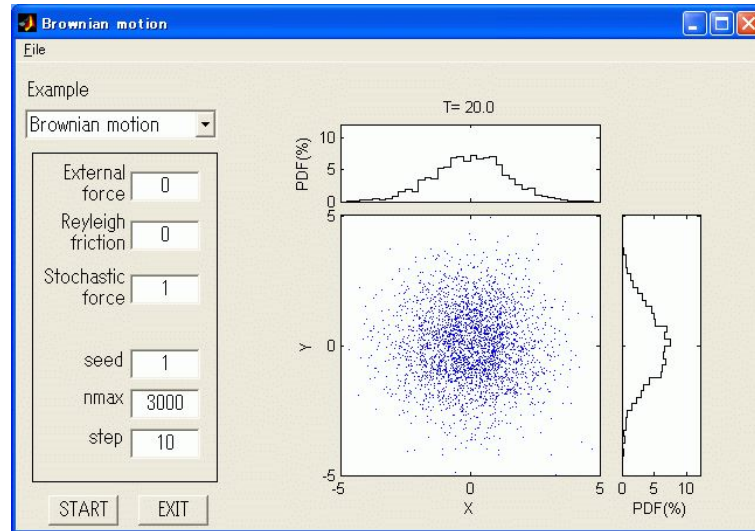Click the graph window or the NEXT button, and new results for different random sequences will be shown (for 9 times).

Figure 5.2: Result of Example 2.

Change the value of `External force` or `Rayleigh friction`, and plot graphs to observe the difference of particle tracks among various cases. It can be seen that each particle oscillates randomly, and is drifted by external force. Put a nonzero integer into `seed`, and you can assign another sequence of deviates for calculation.

Each of particles shows random track independently, and these particle motions depend not on the past status but on what happened last. This stochastic process is called *Markov process* [e.g. *Kitahara*, 1997; section 4-6].

Example 2 Particle diffusion process

Run "C5-2" to observe the behavior of 3000 particles. For the initial condition, particles are distributed uniformly in a circle in the center. Same as "C5-1", set both parameters 0 for default, and begin test with the basic condition.

Click the `START`, and you can see the movie of particle motions.

The particles, which are localized in the initial condition, become spatially expanded gradually, and the particle distribution function projected on each axis becomes like a Gaussian distribution. Random oscillation of each particles give rise to *diffusion process*.

Change the parameters, and compare the difference of particle diffusion processes in various conditions. Set the parameter `step` smaller, if you want to change the time resolution of plot output higher.

References

Kitahara, K., 1997: *Nonequilibrium statistical mechanics*, Iwanami Basic Series in Physics 8, Iwanami Shoten Publishers, 279pp (in Japanese).

Kobayashi, K., 1983: *Thermal Statistical Physics I*, Asakura Shoten Publishers, 239pp (in Japanese).

Rodean, H.C., 1996: *Stochastic Lagrangian models of turbulent diffusion*, Meteorological Monographs **26 (No.48)**, American Meteorological Society, 84pp.

Chapter 6

Two-Dimensional System of Vortex Filaments

In this chapter, we discuss interaction and motion of vortices which are close to each other in the two-dimensional ideal fluid. For simplicity, each vortex is idealized to *a vortex filament*, whose vorticity is concentrated in a line (a point on the two-dimensional plane). The vortex filaments can be regarded as the singular points in a non-rotational flow of the non-divergent ideal fluid. The velocity field induced by one vortex filament is derived analytically. The velocity field induced by a group of vortex filaments is the sum of the velocity fields induced by each vortex filament. The motion of the vortex filaments is governed by the velocity field. We can analytically solve the motion of the vortex filaments in the system of two vortex filaments. In the system of more-than-two vortex filaments, the motion of the vortex filaments is generally solved through numerical integration of the governing equations. More detailed discussion of the following theoretical issues is in Tatsumi (1982; subsection 9-3).

6.1 Theoretical Background

6.1.1 Motion of the system of vortex filaments

The flow induced by one vortex filament is one of the two-dimensional potential flows which is defined as a non-rotational flow of the non-divergent ideal fluid (Tatsumi, 1982; subsection 8-2-4). We can define a complex velocity potential, W, of a non-rotational flow induced by a vortex filament located at the origin as

$$W = -i\kappa \log z = \kappa\theta - i\kappa \log r, \tag{6.1}$$

where $z = re^{i\theta}$, (r, θ) is the polar coordinates, and κ is a real constant. The complex velocity potential can be represented as $W = \Phi + i\Psi$ where Φ is the velocity potential and Ψ the stream function. The stream line of this flow is, therefore, a group of concentric circles whose centers are at the origin. The radial component of the flow, u_r, is zero. The tangential component of the flow $,u_\theta$, is

$$u_\theta = \frac{1}{r}\frac{\partial \Phi}{\partial \theta} = \frac{\kappa}{r}. \tag{6.2}$$

The circulation Γ along any closed curve which encloses the origin is

$$\Gamma = 2\pi\kappa. \tag{6.3}$$

We can represent the above velocity field also in the Cartesian coordinates (x, y). The complex velocity, $w \equiv u - iv$, where (u, v) represent the velocity field, is given by

$$w = \frac{dW}{dz}, \tag{6.4}$$

where $z = x + iy$.

Consider the velocity field induced by N vortex filaments in the two-dimensional Cartesian coordinates. The complex velocity potential of the flow induced by the N vortex filaments is given by

$$W = \frac{1}{2\pi i} \sum_{n=1}^{N} \Gamma_n \log(z - z_n), \tag{6.5}$$

where Γ_n is the circulation which n-th vortex filament has, and (x_n, y_n) is the circulation of the n-th vortex filaments. Substitution (6.5) for (6.4) gives us the complex velocity at any point z.

The velocity of m-th vortex filament, which is induced by the other vortex filaments, is given by

$$\frac{dz_m^*}{dt} = w_m = \left[\frac{d}{dz} \left(W - \frac{\Gamma_m}{2\pi i} \log(z - z_m) \right) \right]_{z=z_m} = \frac{1}{2\pi i} \sum_{n=1, n \neq m}^{N} \frac{\Gamma_n}{z_m - z_n}, \tag{6.6}$$

where $<>^*$ denotes the complex conjugate of $<>$. The N complex simultaneous equations (6.6) can describe completely the motion of the system of the N vortex filaments.

6.1.2   The Hamilton function of the system of the vortex filaments

Using a real function, H, which depends only on the relative distance between vortex filaments which constitute the system, r_{mn},

$$\left. \begin{array}{l} H = -\frac{1}{4\pi} \sum_{m=1}^{N} \sum_{n=1, m \neq n}^{N} \Gamma_m \Gamma_n \log r_{mn}, \\ r_{mn} = |z_m - z_n| = \sqrt{(x_m - x_n)^2 + (y_m - y_n)^2}, \end{array} \right\} \tag{6.7}$$

we can represent the equations of motion of the system (6.6) as

$$\Gamma_m \frac{dz_m^*}{dt} = 2i \frac{\partial H}{\partial z_m}. \tag{6.8}$$

Decomposition of (6.8) into real and imaginary parts yields

$$\Gamma_m \frac{dx_m}{dt} = \frac{\partial H}{\partial y_m}, \qquad \Gamma_m \frac{dy_m}{dt} = -\frac{\partial H}{\partial x_m}. \tag{6.9}$$

For the derivation of (6.9), we use a relation $\frac{\partial}{\partial z} = \frac{1}{2} \left(\frac{\partial}{\partial x} - i \frac{\partial}{\partial y} \right)$. Equation (6.9) is *a Hamilton's canonical equation* with canonical variables x_m and y_m, and H is *a Hamiltonian*.

General features of the system of the vortex filaments are summarized as follows.

- Function H only depends on the relative distance r_{mn}, and is invariant under translation and rotation of the system.

- In case of $\sum \Gamma_m \neq 0$, the center of the gravity of the system, $z_0 \equiv \sum_{m=1}^{N} \Gamma_m z_m / \sum_{m=1}^{N} \Gamma_m$, is stationary.

- In case of $\sum \Gamma_m = 0$, if the vortex filaments are divided into any two groups, the relative distance of the centers of the gravity of them is constant.

- The moment of inertia of the system with respect to the origin, $I \equiv \sum_{m=1}^{N} \Gamma_m(x_m^2 + y_m^2)$, is constant.

- The angular momentum of the system with respect to the origin, $A \equiv \sum_{m=1}^{N} \Gamma_m(x_m dy_m/dt - y_m dx_m/dt)$, is constant.

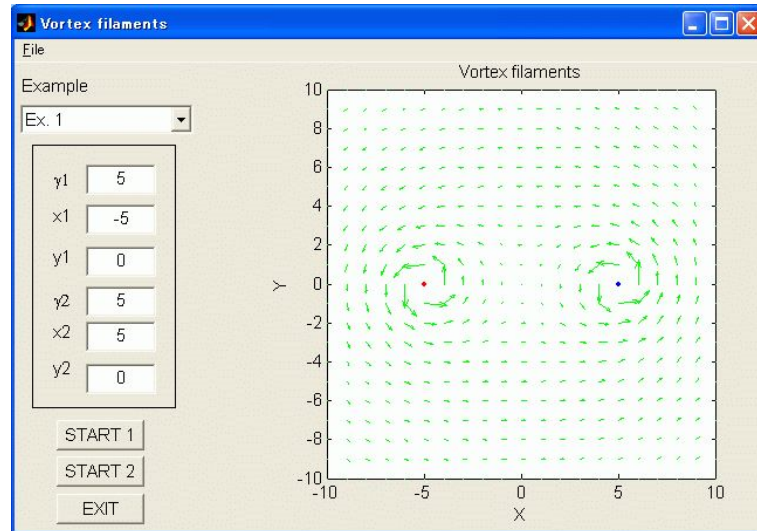- Function H is independent of time.

Figure 6.1: Result of Example 1.

6.2 Exercises

6.2.1 The flow induced by the system of vortex filaments

The program "C6-1&2" visualizes the flow induced by two vortex filaments and their motion. Velocity at any point (x, y) is derived from (6.4) and (6.5).

Example 1 The flow induced by two vortex filaments.

$$
\begin{array}{cccccc}
5.0 & -5.0 & 0.0 & 5.0 & 5.0 & 0.0 \\
\gamma 1 & x1 & y1 & \gamma 2 & x2 & y2
\end{array}
$$

Parameters $\gamma 1$ and $(x1,y1)$ represents the circulation and the position of the vortex filament 1, respectively. Parameters $\gamma 2$ and $(x2,y2)$ represents the same except for the vortex filament 2. *START 1* of the program *uzuito_ui* first shows the flow induced by the vortex filament 1, a few seconds later the flow induced by the vortex filament 2. After next few seconds, it shows the flow which is induced by these two vortex filaments. Change strengths and signs of the circulation and the relative distance of these vortex filaments to examine how flow is induced.

6.2.2 Motion of the system of two vortex filaments

In case of the system of two vortex filaments, the Hamiltonian (6.7) of the system is expressed as

$$
H = -\frac{1}{2\pi}\Gamma_1\Gamma_2 \log r_{12} = constant, \tag{6.10}
$$

and thus the distance between the vortex filaments, r_{12}, is turned out to be constant value of d. If $\Gamma_1 + \Gamma_2 \neq 0$, the center of the gravity of the system is stationary. In this case, two vortex filaments rotate with constant speeds along circles which center is the center of the gravity of the system. The center of the gravity (x_0, y_0) is

$$
(x_0, y_0) = \left(\frac{\Gamma_1 x_1 + \Gamma_2 x_2}{\Gamma_1 + \Gamma_2}, \frac{\Gamma_1 y_1 + \Gamma_2 y_2}{\Gamma_1 + \Gamma_2}\right). \tag{6.11}
$$

The angular momentum of the system is constant. The two vortices rotate around their center of the gravity with a constant angular velocity. Such motion of these vortices is a kind of *the Fujiwara effect* since a vortex with positive circulation is a good model of typhoon.

the Fujiwara effect : When two typhoons are close to each other, their motion is complicated because of their interaction. This is called *the Fujiwara effect*. Their ideal relative motion is that they rotate anti-clockwise (clockwise in the Southern Hemisphere) around a certain point between the typhoons. Sometimes one typhoon decelerates to become almost stationary while the other accelerates. In reality, the Fujiwara effect is recognized when the distance of two typhoons are less than 800 km. This effect was advocated by Sakuhei Fujiwara who had served as a director of the Japan Meteorological Agency. (Encyclopedia of Meteorology and Atmospheric Sciences, 1998)

On the other hand, when $\Gamma_1 + \Gamma_2 = 0$, i.e. $\Gamma_1 = -\Gamma_2 = \Gamma$, the center of the gravity can not be defined. Two vortex filaments move with the same velocity,

$$\frac{dz_1}{dt} = \frac{dz_2}{dt} = \frac{1}{2\pi i} \frac{\Gamma}{z_2^* - z_1^*}. \tag{6.12}$$

Such *vortex pair* moves with speed of $\Gamma/(2\pi d)$ and the direction perpendicular to the straight line which connects these vortex filaments.

Substituting (6.10) to (6.9) yields

$$\begin{cases} \frac{dx_1}{dt} = & \frac{1}{\Gamma_1}\frac{\partial H}{\partial y_1} = & -\frac{\Gamma_2}{2\pi}\frac{y_1 - y_2}{d^2}, \\[2mm] \frac{dy_1}{dt} = & -\frac{1}{\Gamma_1}\frac{\partial H}{\partial x_1} = & \frac{\Gamma_2}{2\pi}\frac{x_1 - x_2}{d^2}, \\[2mm] \frac{dx_2}{dt} = & \frac{1}{\Gamma_2}\frac{\partial H}{\partial y_2} = & \frac{\Gamma_1}{2\pi}\frac{y_1 - y_2}{d^2}, \\[2mm] \frac{dy_2}{dt} = & -\frac{1}{\Gamma_2}\frac{\partial H}{\partial x_2} = & -\frac{\Gamma_1}{2\pi}\frac{x_1 - x_2}{d^2}. \end{cases} \tag{6.13}$$

The motion of the vortex filaments are solved with integration of the above simultaneous ordinary differential equations.

Example 2 The system of two vortex filaments

5.0	-5.0	0.0	5.0	5.0	0.0
$\gamma 1$	x1	y1	$\gamma 2$	x2	y2

These parameters are the same as that of Example 1. Two vortices which have the same value of the circulation rotate along a circle which center is the intermediate point between the vortices. The direction of the motion of the vortices is, of course, the same as the direction of the vortices.

If the intensity of the circulation of the two vortices are different each other and the signs of them are the same, the center of the gravity of them is the point which divide r_{12} internally to $\Gamma_2 : \Gamma_1$. These two vortices rotate along circles which centers are at the center of the gravity. This is so-called the Fujiwara effect. Change Γ_2 to examine how the position of the center of the gravity changes.

In case of the vortex pair, the center of the gravity can not be defined. The vortex filaments move with the same velocity each other toward the direction perpendicular to the straight line which connects the vortex filaments. Confirm the relationship between the direction of the rotation of the vortices and the direction of their motion.

If two vortex filaments have different intensity and different signs of the circulation, the center of the gravity of them is the point which divide r_{12} externally to $\Gamma_2 : \Gamma_1$. The vortex filaments rotate along circles which centers are at the center of the gravity. Change Γ_2 to examine how the position of the center of the gravity changes.
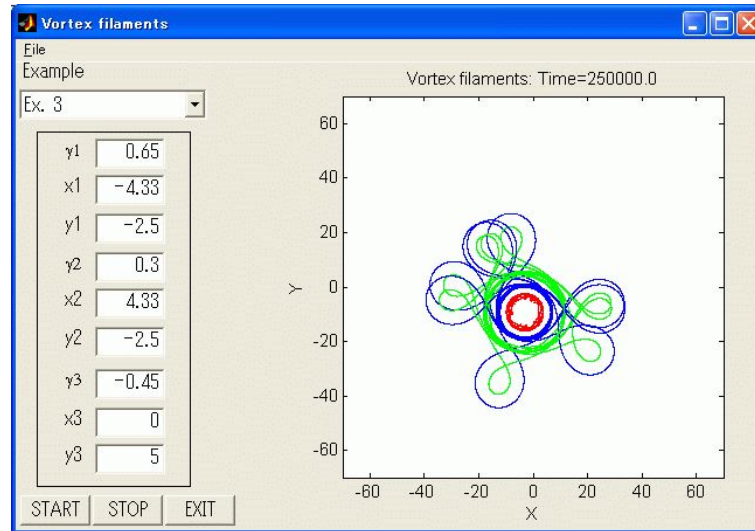
Figure 6.2: Result of Example 3.

6.2.3   The system of three vortex filaments

We can solve the motion of the system of three vortex filaments analytically only if they have the same value of the circulation, Γ and locate at vertices of a equilateral triangle (see the next subsection). Like the system of two vortex filaments, three vortex filaments move along various loci which depend on the sign and intensity of their circulation and the position of them.

Example 3 The system of three vortex filaments.

$$
\begin{array}{ccccccccc}
0.65 & -4.33 & -2.5 & 0.3 & 4.33 & -2.5 & -0.45 & 0.0 & 5.0 \\
\gamma1 & \text{x1} & \text{y1} & \gamma2 & \text{x2} & \text{y2} & \gamma3 & \text{x3} & \text{y3}
\end{array}
$$

The program "C6-3" visualizes the loci of three vortex filaments. In its graphics, the red, blue, and green points indicate location of the vortex filaments which have the circulation of $\gamma1$, $\gamma2$, $\gamma3$, respectively. The system of three vortex filaments whose signs of the circulation are different each other can move along chaotic loci. This chaotic motion is not observed in the system of two vortex filaments.

On the other hand, three vortex filaments have the same value of the circulation and locates in equal distance (vertices of a equilateral triangle), they rotate along the same circle apart 120 degrees each other. When three vortex filaments which have the same value of the circulation locate on a straight line at regular intervals, the central filament is motionless while the others rotate along the same circle which center is at the central filament. Examine how motion changes in these cases when position of a vortex filament change slightly.

Examine how is the motion of three vortex filaments which circulation are the same signs but different intensity. Is the motion chaotic?

Examine how is the motion of three vortex filaments which circulation are the same intensity but different signs. How is the motion of three vortex filaments if two vortex filaments which circulation are the same sign are located closely to each other while the other which circulation is the different sign is located apart? How is the motion of three vortex filaments if two vortex filaments which circulation are the opposite signs to each other are located closely while the other is located apart ?

Change the circulation and initial position of the vortex filaments in various ways to examine the motion.

6.3 Appendix

Examine analytically the motion of three vortex filaments which have the same value of the circulation, Γ, and are located at the vertices of a equilateral triangle. Derive the Hamiltonian of the system and the equations of motion to confirm that the vortex filaments rotate along the same circle which center is at the center of the gravity of them. You can also discuss the stability of the circular motion.

References

GEFD Summer School, 1994: Demonstration 5: Point vortices. *Computer Demonstration Note.*

Meteorological Society of Japan (edit.), 1998: Encyclopedia of Meteorology and Atmospheric Sciences, Tokyo Shoseki, 637pp (in Japanese).

Tomomasa Tatsumi, 1982: Fluid Mechanics, Baifukan, 453pp (in Japanese).

Chapter 7

Inertial Oscillation and Inertial Instability

Motion of a free particle on a rotating frame of reference without the effect of the centrifugal force, which results from the rotation of the frame, is periodic and termed the inertial oscillation. We can discuss stability of sheared flow on the same rotating frame of reference with the parcel method. The stability results from a relationship between the shear of the flow and the Coriolis force.

7.1 Theoretical Background

7.1.1 Inertial oscillation

The equation of motion of a free particle on a plane rotating with a constant angular velocity Ω is given by

$$\frac{du}{dt} - fv = 0, \tag{7.1}$$

$$\frac{dv}{dt} + fu = 0, \tag{7.2}$$

where $f \equiv 2\Omega$ is the Coriolis parameter, while the centrifugal force is neglected. Eliminating v from (7.1) and (7.2), we obtain

$$\frac{d^2u}{dt^2} + f^2u = 0. \tag{7.3}$$

This ordinary differential equation (7.3) can be integrated with the initial condition of $u = u_0$ and $v = v_0$ at $t = 0$,

$$u(t) = u_0 \cos ft + v_0 \sin ft. \tag{7.4}$$

By similar procedure,

$$v(t) = u_0 \sin ft + v_0 \cos ft. \tag{7.5}$$

Integration of (7.4) and (7.5) with the initial condition of $x = x_0$ and $y = y_0$ at $t = 0$ yields

$$x(t) = \frac{v_0}{f}(1 - \cos ft) + \frac{u_0}{f} \sin ft + x_0, \tag{7.6}$$

$$y(t) = -\frac{u_0}{f}(1 - \cos ft) + \frac{v_0}{f} \sin ft + y_0. \tag{7.7}$$

We can easily find from solutions (7.6) and (7.7) that the motion of the free particle is periodic with its period (inertial period) of $2\pi/f$, which is a half of the period of the frame's rotation, $2\pi/\Omega$, and with its direction reverse to the direction of the frame's rotation.

7.1.2 Inertial instability

We discuss the stability of two-dimensional flow on the rotating frame of reference. More detailed discussion is given in Yoden (1998; subsection 10.3). If the pressure gradient has only y-component, the basic state field of the flow is a zonally directed geostrophic wind $\overline{u}_g(y)$ which is independent of x,

$$\overline{u}_g(y) = -\frac{1}{\rho f}\frac{\partial p}{\partial y}. \tag{7.8}$$

Here we study a motion of a parcel on this field. Since we assume that the parcel displacement does not disturb the pressure field, the background geostrophic wind is stable. The equations of motion of the parcel are given by

$$\frac{Du}{Dt} = fv, \tag{7.9}$$

$$\frac{Dv}{Dt} = -fu - \frac{1}{\rho}\frac{\partial p}{\partial y} = -f\left\{u - \overline{u}_g(y)\right\}, \tag{7.10}$$

where $u = Dx/Dt$ and $v = Dy/Dt$. If the parcel is displaced along y direction by a distance δy, parcel's new u is derived through integration of (7.9),

$$u(y_0 + \delta y) = \overline{u}_g(y_0) + f\delta y. \tag{7.11}$$

On the other hand, the geostrophic wind at $y = y_0 + \delta y$ can be approximated as

$$\overline{u}_g(y_0 + \delta y) = \overline{u}_g(y_0) + \frac{d\overline{u}_g}{dy}\delta y. \tag{7.12}$$

Using (7.11) and (7.12), we have the y-component of the equation of motion of the parcel (7.10) at $y = y_0 + \delta y$ as

$$\frac{Dv}{Dt} = -f\left(f - \frac{d\overline{u}_g}{dy}\right)\delta y. \tag{7.13}$$

Introducing an absolute momentum $M \equiv fy - \overline{u}_g$ to (7.13), we obtain

$$\frac{D^2}{Dt^2}(\delta y) = -f\frac{dM}{dy}\delta y. \tag{7.14}$$

Equation (7.14 enables us to discuss the stability of the geostrophic wind $\overline{u}_g$. If $f\frac{dM}{dy}$ is positive, δy only oscillates with the period of $2\pi(f\frac{dM}{dy})^{-1/2}$ and thus the geostrophic wind $\overline{u}_g$ is stable. On the other hand, if $f\frac{dM}{dy}$ is negative, δy leaves from the original value exponentially with time, and thus the geostrophic wind $\overline{u}_g$ is unstable. In summary, the condition for the inertial instability is

$$\begin{cases} fdM/dy > 0 & stable, \\ fdM/dy = 0 & neutral, \\ fdM/dy < 0 & unstable. \end{cases} \tag{7.15}$$

In the case that the background geostrophic wind is expressed as

$$\overline{u}_g(y) = py + q, \tag{7.16}$$

we can solve (7.9) and (7.10) with the initial condition of $(x, y, u, v) = (x_0, y_0, u_0, v_0)$ at $t = 0$ as follows.

i) when $f \, dM/dy > 0 (f > p$, stable),

$$x(t) \ = \ \frac{1}{f-p}\left\{(1-\cos\omega t)v_0 - f(t-\frac{1}{\omega}\sin\omega t)(u_0-u_g)\right\} + u_0 t + x_0, \qquad (7.17)$$

$$y(t) \ = \ -\frac{1}{f-p}(1-\cos\omega t)(u_0-u_g) + \frac{v_0}{\omega}\sin\omega t + y_0, \qquad (7.18)$$

where

$$\omega = \sqrt{f(f-p)}, \qquad (7.19)$$

ii) when $f \, dM/dy = 0 \ (f = p$, neutral),

$$x(t) \ = \ -\frac{f^2}{6}(u_0-u_g)t^3 + \frac{1}{2}v_0 f t^2 + u_0 t + x_0, \qquad (7.20)$$

$$y(t) \ = \ -\frac{f}{2}(u_0-u_g)t^2 + v_0 t + y_0, \qquad (7.21)$$

iii) when $f \, dM/dy < 0 \ (f < p$, unstable),

$$x(t) \ = \ \frac{1}{2(p-f)}\left\{v_0 - \frac{f}{r}(u_0-u_g)\right\}e^{rt} + \frac{1}{2(p-f)}\left\{v_0 + \frac{f}{r}(u_0-u_g)\right\}e^{-rt}$$
$$+ \frac{f}{p-f}(u_0-u_g)t + u_0 t + x_0 - \frac{1}{p-f}v_0, \qquad (7.22)$$

$$y(t) \ = \ \frac{1}{2r}\left\{v_0 - \frac{f}{r}(u_0-u_g)\right\}e^{rt} + \frac{1}{2r}\left\{v_0 + \frac{f}{r}(u_0-u_g)\right\}e^{-rt}$$
$$+ \frac{1}{p-f}(u_0-u_g) + y_0, \qquad (7.23)$$

where

$$r = \sqrt{f(p-f)}. \qquad (7.24)$$

In the above solutions, u_g implies $\bar{u}_g(y_0)$.

7.2 Exercises

7.2.1 Inertial oscillation

In the rotating frame of reference, the free particle rotates along the inertial circle with the inertial period. The program "C7-1" enables us to visualize a behavior of a free particle viewed not only on rotating frame of reference but also on inertial frame of reference.

Example 1

30.0	0.0	400.0	25.0	0.0
Latitude	X0	Y0	U0	V0

It will be confirmed that the free particle on the rotating frame of reference (top panel) rotates along the inertial circle with a half of the period of frame's rotation. Select the different latitude to examine how the inertial period changes with latitude.
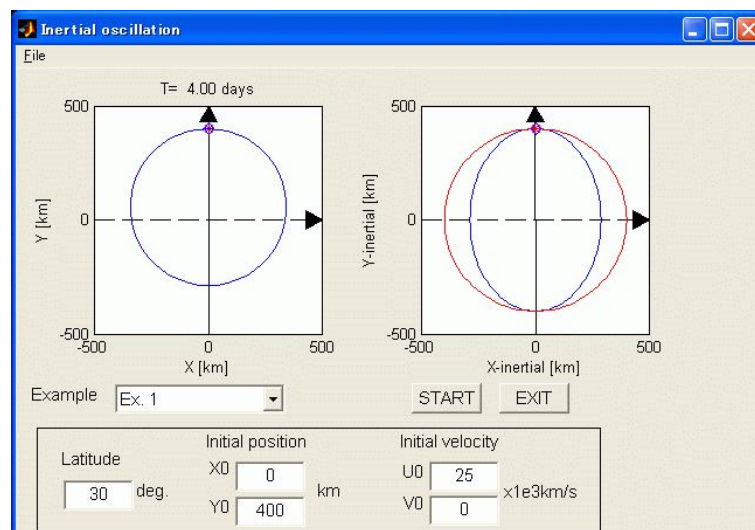
Figure 7.1: Result of Example 1.

7.2.2   Inertial instability

Execute the program "C7-2" to examine the stability of the geostrophic flow which has the meridional shear, p.

Example 2

5.0	0.0	0.0	12.676	0.0	18.984	0.0	50.0
Lat.	p1	q1	p2	q2	p3	q3	dy

In this example, the flow is stable (top panel), neutral (middle panel), and unstable (bottom panel). Change *Lat.* or p to examine which condition makes the flow stable (unstable).
Setting all three ps to 0, you can observe the inertial oscillation in three cases of uniform background zonal flow.

Example 3

30.0	0.0	0.0	0.0	5.0	0.0	10.0	100.0
Lat.	p1	q1	p2	q2	p3	q3	dy

Note that the periods of three cases in the example 3 are the same each other.

7.3   Appendix

To understand the inertial oscillation in a physical sense, refer to Sakai (1995), Cushman-Roisin (1994) and Durran (1993). Note that consideration to motion of a ball in a bowl is helpful to our understanding of the inertial oscillation.

References

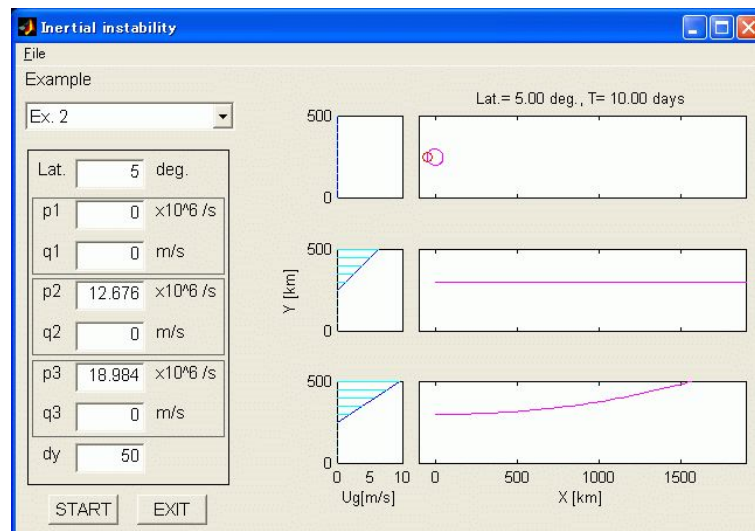Cushman-Roisin, B., 1994:*Introduction to Geophysical Fluid Dynamics*, Prentice-Hall, 16-32.

Figure 7.2: Result of Example 2.

Dale R. Durran, 1993:*Is the Coriolis Force Really Responsible for the Inertial Oscillation?*, America
    Meteorological Society, 2179-2184.

Sakai, S., 1995:*Movies of fundamental experiments of geofluid dynamics* (in Japanese).

Yoden S., 1998:*Meteorology I*, 146pp (in Japanese).

Chapter 8

Inertial Gravitational Wave

Carry out numerical experiments about the inertial gravitational wave to show the difference between its phase velocity and group velocity.

8.1 Theoretical Background

We introduce the Coriolis force into the shallow-water equations as follows,

$$u_t = \quad fv - gh_x \qquad \text{:}x\text{-component of the equation of motion} \tag{8.1}$$

$$v_t = \quad -fu - gh_y \qquad \text{:}y\text{-component of the equation of motion} \tag{8.2}$$

$$h_t = \quad -H(u_x + v_y) \quad \text{:the continuity equation} \tag{8.3}$$

where f is the Coriolis parameter, g the acceleration of gravity, H the depth.

Eliminating u and v yields

$$(\partial^2/\partial t^2 + f^2)\frac{\partial h}{\partial t} = gH(\partial^2/\partial x^2 + \partial^2/\partial y^2)\frac{\partial h}{\partial t} \tag{8.4}$$

Wave solutions which are periodic in x, y and t can be sought in the form

$$h = h_0 \exp\{i(kx + ly - \omega t)\} \tag{8.5}$$

where h_0 is the wave amplitude.

Substitution (8.5) into (8.4) yields

$$\omega\{\omega^2 - f^2 - gH(k^2 + l^2)\}h_0 = 0 \tag{8.6}$$

Thus, a time-periodic flow is obtained only if

$$\omega = \pm\{f^2 + (k^2 + l^2)gH\}^{1/2} \tag{8.7}$$

This condition is called the *dispersion relation*.

When k or l is large enough, f can be neglected so that the solution is identical to the shallow-water wave which is under no influence of the Coriolis force. On the other hand, when $k = l = 0$, it represents the inertial oscillation.

8.2 Phase Velocity and Group Velocity

The velocity with which each crest and trough of the wave advance is called the *phase velocity*. When crests of the wave are parallel to y-axis, the phase velocity C_p is given by

$$C_p = \omega/k \tag{8.8}$$

Meanwhile, the velocity of a 'wave packet', waves traveling in a group or packet, is called the *group velocity*. The group velocity C_g is given by

$$C_g = \partial\omega/\partial k \tag{8.9}$$

The wave energy propagates with the packet at the group velocity.

These two velocities nealy coincide when k, l are large. However, if $\sqrt{k^2 + l^2} < f/\sqrt{gH}$, the difference becomes large. The inverse number of the criterion measure, $\sqrt{gH}/f$, is called the *deformation radius*, i.e. for the wave with larger wavelength than the deformation radius, the group velocity doesn't coincide with the phase velocity.

8.3   Exercises

Though the shallow-water equations are horizontally 2-dimensional, the plane wave can be treated 1-dimensionally by steering the x-axis parpendicular to crest lines of the wave, without loss of generality. It means $\partial/\partial y \equiv 0$, so that the shallow-water equations reduce to

$$
\begin{array}{lll}
u_t = & fv - gh_x & \text{x-component of the equation of motion} \tag{8.10} \\
v_t = & -fu & \text{y-component of the equation of motion} \tag{8.11} \\
h_t = & -Hu_x & \text{the continuity equation} \tag{8.12}
\end{array}
$$

Perform the program named as "C8" in GFD Menu to study time-integration of these governing equations numerically, and observe the difference between the phase velocity and the group velocity.

Example 1 Set the parameters as follows,

$$
\begin{array}{cccc}
1.0 & 1.0 & 0.8 & 5.0 \\
\text{g} & \text{f} & \text{Amp.} & \text{Wave Num.}
\end{array}
$$

Click 'START', the animation (top panel) and the x - t diagram of h (bottom panel) are displayed.
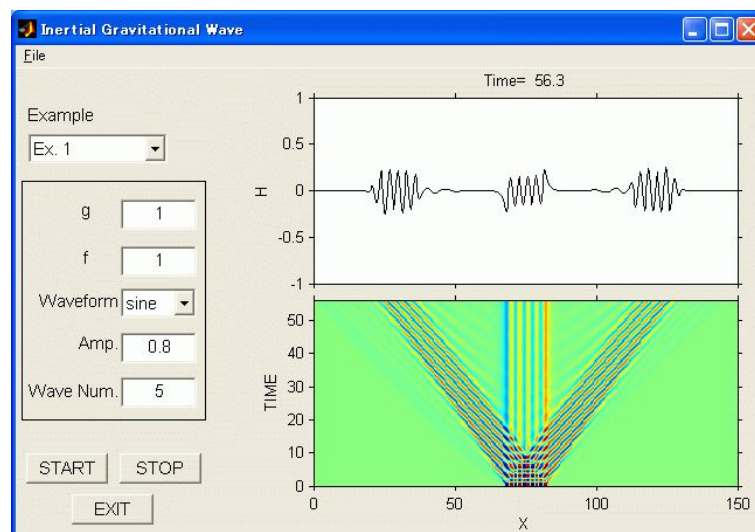
Figure 8.1: Result of Example 1.

Chapter 9

Rossby wave

9.1 Theoretical Background

9.1.1 Basic equations and the dispersion relation of Rossby wave

We assume that the coriolis parameter f is written in the form (9.1).

$$f = 2\Omega sin\phi \approx 2\Omega sin\phi_0 + 2\Omega\frac{y}{a}cos\phi_0 = f_0 + \beta y \tag{9.1}$$

where

$$\phi = \phi_0 + \frac{y}{a} \tag{9.2}$$

The constant Ω is the angular velocity of the planet and ϕ is latitude. The constant ϕ_o is the latitude of the reference state. The constant a is the planetary radius and the variable y is the latitudal displacement from the reference state.

On this β *plane*, the quasi-geostrophic potential vorticity equation is given as (9.3).

$$\frac{\partial}{\partial t}\nabla_H\psi + \frac{\partial(\psi, \Delta_H\psi)}{\partial(x, y)} + \beta\frac{\partial\psi}{\partial x} = 0 \tag{9.3}$$

(see Rhines(2002).)

Eaquation (9.3) is a non-linear partial derivative equation, in which a stream function $\psi(x, y, t)$ is a dependent variable of x, y, and t.

We separate variables into basic state and perturbation. A variable $\overline{\alpha}$ is a basic state of α. A variable α' is a perturbation part of α. We assume a static solution as a basic state.

$$\overline{u} = \overline{v} = 0 \tag{9.4}$$

$$\overline{\psi} = constant \tag{9.5}$$

The stream function ψ is written as (9.6).

$$\psi(x, y, t) = \overline{\psi} + \psi'(x, y, t) \tag{9.6}$$

The basic equation linearized in terms of perturbation $\psi'(x, y, t)$ is (9.7).

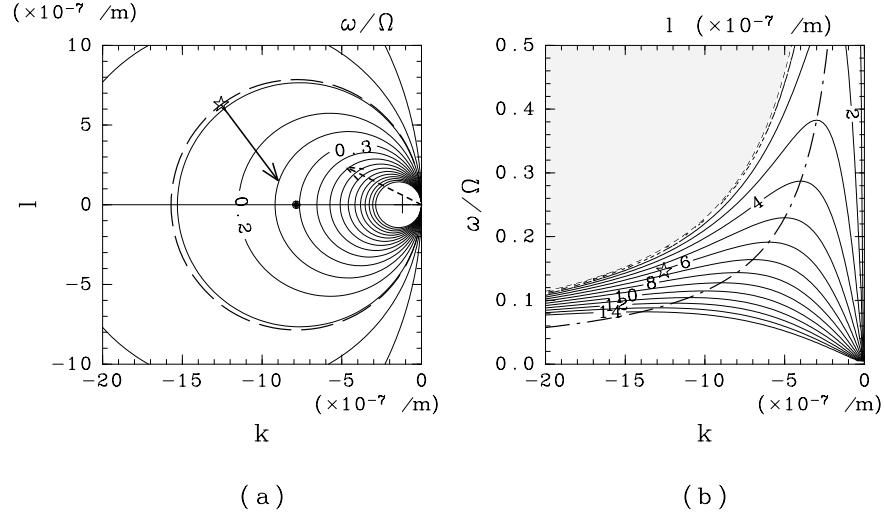$$\frac{\partial}{\partial t}\nabla_H\psi' + \beta\frac{\partial\psi'}{\partial x} = 0 \tag{9.7}$$

Figure 9.1: Dispersion relation of two-dimensional non-diverce Rossby wave on a β plane. (a) Non-dimensionalized ω by Ω as a function of non-dimensionalized wavenumber $(k, l)a$ by planetaly radius "a". Bold dashed arrow is phase velocity in real space. Bold solid arrow is group velocity in real space. (b) Meridional wavenumber la as a function of ka and ω/Ω. Shade represents area of $l^2 < 0$. We will show a structure of Rossby wave marked as $\star$ in fig. 9.2.

We assume periodicity in time and space. Give a sine wave solution as (9.8).

$$\psi'(x, y, t) = Re\left[\Psi_0 e^{i(kx+ly-\omega t)}\right] \tag{9.8}$$

Substituting (9.8) into (9.7), we obtain the dispersion relation of two-dimensional *Rossby wave* on a β plane.

$$\omega = -\frac{\beta k}{k^2 + l^2} \tag{9.9}$$

Because $\beta > 0$, the sign of ω and that of k is always different. Figure 9.1 shows the dispersion relation. In fig. 9.1, wavenumber and frequency is non-dimensionalized by a^{-1} and Ω, respectively. Figure 9.1(a) shows non-dimensionalized freqency ω/Ω in terms of non-dimensionalized wavenumber (ka, la), where $\omega > 0$. Equation (9.9) can be translated into an equation below.

$$\left(k + \frac{\beta}{2\omega}\right)^2 + l^2 = \left(\frac{\beta}{2\omega}\right)^2 \tag{9.10}$$

This equation represents circle-shape when we take a line where ω is a constant. The center of the circle is located $(-\beta/2\omega, 0)$, and the radius of it is $\beta/2\omega$. As ω increases, the radius of the circle decreases and approaches the origin. Figure 9.1(b) shows non-dimensionalized meridional wavenumber la in terms of ka and ω/Ω. In shaded area, while $\omega > -\beta/k$, l becomes pure imaginary number. In this case, there is no solution of meridionaly propagationg sine wave. The wave solution in this case is an external wave with an exponential structure in space.

From dispersion relation (9.9), the phase velocity (c_{px}, c_{py}) and the group velocity (c_{gx}, c_{gy}) of
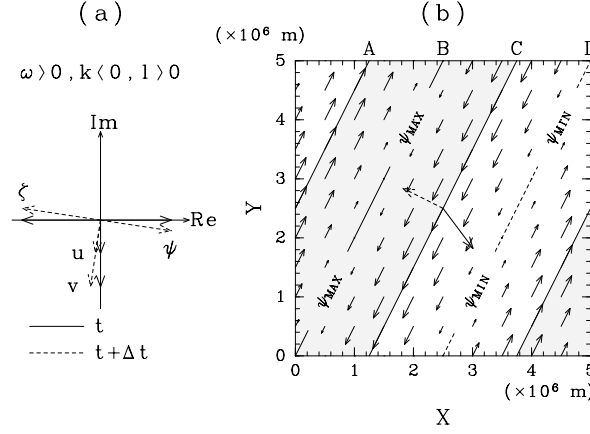
Figure 9.2: (a) Phase relation of Rossby wave (In case of $\omega > 0, k < 0, m > 0$; At the point of $\star$ in fig. 9.1). (b) Spacial structure of Rossby wave at t in (a). Dashed arrow shows phase velocity and Bold arrow shows group velocity. Solid arrows represent velocity field of fluid. Area of $\zeta' < 0$ is shaded.

Rossby wave are calculated as shown in (9.11) - (9.14).

$$c_{px} = \frac{\omega}{k} = -\frac{\beta}{k^2 + l^2} \tag{9.11}$$

$$c_{py} = \frac{\omega}{l} = -\frac{k}{l}\frac{\beta}{k^2 + l^2} \tag{9.12}$$

$$c_{gx} = \frac{\partial \omega}{\partial k} = \frac{\beta(k^2 - l^2)}{(k^2 + l^2)^2} \tag{9.13}$$

$$c_{gy} = \frac{\partial \omega}{\partial l} = \frac{2\beta kl}{(k^2 + l^2)^2} \tag{9.14}$$

Because $c_{px} < 0$, the phase of this wave always goes west. The sign of the group velocity changes as the sign of $(k^2 - l^2)$ changes. If $(k^2 - l^2) > 0$, $c_{gx} > 0$. If $(k^2 - l^2) < 0$, $c_{gx} < 0$. This means that when the direction of the wave front is near south-north, the wave energy goes east. When the direction of it is near east-west, the wave energy goes west.

When the solution is written as (9.8), the phase relationship among velocity, vorticity, and stream function is written as (9.15) - (9.17).

$$u' = -\frac{\partial \psi'}{\partial y} = -il\psi' \tag{9.15}$$

$$v' = \frac{\partial \psi'}{\partial x} = ik\psi' \tag{9.16}$$

$$\zeta' = \Delta\psi' = -(k^2 + l^2)\psi' \tag{9.17}$$

Since the direction of motion is perpendicular to that of wave propagation, i.e., $\mathbf{u} \cdot \mathbf{k} = 0$ or $\mathbf{u} \cdot \mathbf{c} = 0$, this kind of Rossby wave is a transverce wave.

Figure 9.2(a) shows the phase relation of Rossby wave marked $\star$ in Figure 9.1. Figure 9.2(b) shows spacial structure of the wave. Because $k < 0$ and $l > 0$, iso-phase line of $kx + ly = constant$ slopes upwards going from left to right. The phase of u' is the same as that of v', which is faster than that of ψ' by $\pi/2$. The phase of vorticity is reverse of that of ψ'.

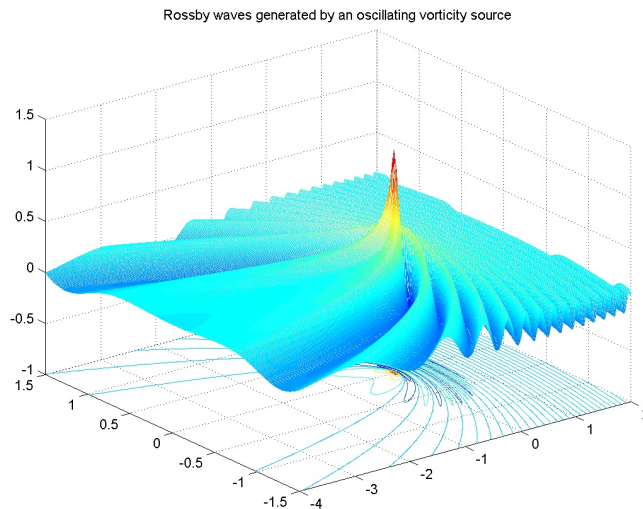Rossby waves generated by an oscillating vorticity source

Figure 9.3: Rossby wave generated by an oscillating vorticity source (Rhines,2002). Seen from southeast of the forcing region.

Figure 9.3 shows the wave pattern of Rossby wave generated by an oscillating vorticity source. Iso-phase line is horseshoe-shaped.

9.2 Exercises

Perform the program "C9" with two types of initial conditions.

Example 1 Wave packet

$$
\begin{array}{cc}
1.0 & 2.0 \\
\beta & k
\end{array}
$$

To run this experiment, click "start1" button.

At an initial time, a wave packet is located at the center of the region. During the calculation, the wave packet goes west. The wave packet is reflected when it reaches boundaries.

We can change β and the wave number in x direction, k. As β or k changes, both phase verosity and group verosity change.

Example 2 Gaussian

$$
\begin{array}{cc}
1.0 & 2.0 \\
\beta & k
\end{array}
$$

At an initial time, a gaussian-shaped height anomaly is located at the center of the field. As time goes, the anomaly is reformed into a horseshoe shape. In this experiment the calculation field is larger than the field we can see on the screen in order to prevent reflection of the wave at boundaries.

We can change β and the width of the gaussian-shaped anomaly k.
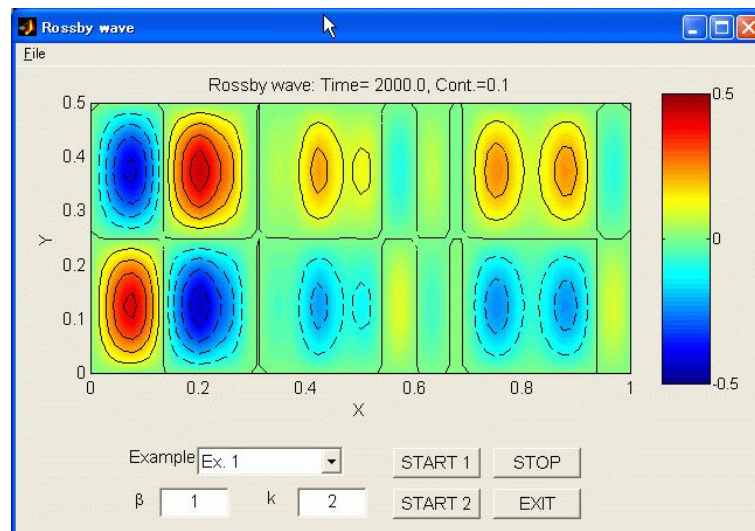
To run this experiment, click "start2" button.

Figure 9.4: Result of Example 1.

Reference

Rhines, 2002 : *Rossby waves*, Encyclopedia of Atmospheric Sciences, Academic Press (available at http://www.ocean.washington.edu/research/gfd/Rossby-final-prfdt-.pdf).

Chapter 10

Parcel Method − Static Instability

Parcel method is a method of testing for instability. In this method, we assume that a displacement is made from a steady state, and only the parcel or parcels displaced are affected, while the environment remaining unchanged. Here, using the parcel method, we study a problem related to static stability in the gravity field.

10.1   Theoretical Background

In this chapter, the incompressible ideal fluid is considered (Yoden, 2000). We assume that the Z-axis is positive upward for the coordinate system and the density distribution for the fluid is $\bar{\rho}(z)$. While a force of gravity $-\bar{\rho}g$ is applied to each unit volume of the fluid (parcel), a pressure gradient force that has the same magnitude as the gravity is applied to the parcel. This leads to the *hydrostatic stability* given by

$$\frac{\partial p}{\partial z} = -\bar{\rho}g. \tag{10.1}$$

Taking this parcel out from the fluid layer and putting a parcel with density ρ instead of it, we find that this parcel is applied by a force of buoyancy of $(\bar{\rho} - \rho)g$. The direction of the buoyancy is upward when $\bar{\rho} > \rho$, and downward when $\bar{\rho} < \rho$.

We assume that a parcel of the unit volume makes a displacement of δz along the z-direction, while the field surrounding the parcel is not disturbed by the displacement of the parcel. If the density difference between the parcel and the surrounding field is $\delta\rho$ and $\delta\rho = -(d\rho/dz)\delta z$, since the buoyancy force is $-g\delta\rho$, the dynamic equation for the parcel can be given by

$$\rho\frac{d^2}{dt^2}(\delta z) = g\frac{d\bar{\rho}}{dz}\delta z. \tag{10.2}$$

When $N^2 \equiv -g\frac{d\bar{\rho}}{dz}$, (10.2) can be written as follows.

$$\frac{d^2}{dt^2}(\delta z) + N^2\delta z = 0 \tag{10.3}$$

Firstly, when $N^2 > 0$, the general solution for (10.3) is given by

$$\delta z = Ae^{iNt} + Be^{-iNt}, \tag{10.4}$$

where coefficient A and B are defined by the initial conditions (the initial location and velocity of the parcel), respectively. Under these conditions, the parcel will vibrate at equilibrium position at angular frequency N. Therefore, when the density decreases vertically as $d\rho/dz < 0$, the field is stable; this kind of status is called *static stability*, and this kind of stratification is called *stable*
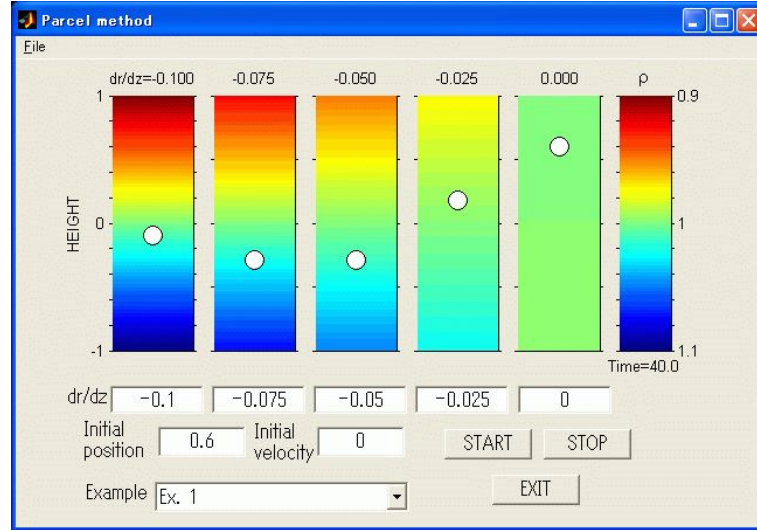
Figure 10.1: Result of stasta

stratification. The angular frequency of N is called *buoyancy frequency* or *brunt vaisala frequency*, which is used as an index for the magnitude of the density stratification.

Secondly, when $N^2 < 0$, the general solution for (10.3) becomes

$$\delta z = Ae^{Nt} + Be^{-Nt}. \tag{10.5}$$

Under this condition, buoyancy force increases the displacement of the parcel. When the density increases vertically as $d\rho/dz < 0$, the parcel will exponentially move away from the equilibrium position as the time lapsed. The field is thus unstable; this kind of status is called *static instability*, while this kind of stratification is called *unstable stratification*. Under such condition, generally, it is not that only one parcel makes displacement and the left part keeps the unchanged status, but all of the elements of the flow affect by each other and make mass motion. This kind of mass motion is generally called *convection*.

On the other hand, when $N^2 = 0$, the general solution for $\dfrac{\delta^2}{\delta t^2}(\delta z) = 0$ becomes

$$\delta z = c_1 t + c_2, \tag{10.6}$$

where c1 and c2 are decided by initial conditions of the parcel. Since the density of the flow does not vary with the height, we find that the parcel will move at a constant velocity. Obviously, when the initial velocity is equal to 0, the parcel stays at the initial position; this kind of status is called *static neutral*.

10.2   Exercises

Since the motion of the parcel is totally decided by its initial displacement, its initial velocity, and density gradient of the surrounding field, we can repeat the experiment by changing these values. The condition-setting parameters for experiments have already been prepared in the program "C10" in GFD Menu. After opening the program, we can adjust the density gradient, initial position and initial velocity for the parcel to watch the results.

Example 1 stable stratification (positive displacement)

Set the coefficients as follows:

0.6	0.0	-0.1	-0.075	-0.05	-0.025	0.0
Initial position	Initial velocity	dr/dz(1)	dr/dz(2)	dr/dz(3)	dr/dz(4)	dr/dz(5)

When the density gradient $d\bar{\rho}/dz < 0$, the parcel will vibrate. The vibration period is shorter as the stratification is stronger (left side). Because the initial velocity is 0, in neutral density stratification, the parcel will stop at the point where the displacement is finished.

Example 2 unstable stratification (positive displacement)

Set the coefficients as follows:

0.3	0.0	0.1	0.075	0.05	0.025	0.0
Initial position	Initial velocity	dr/dz(1)	dr/dz(2)	dr/dz(3)	dr/dz(4)	dr/dz(5)

When a density gradient is assumed, the parcel will exponentially moves away from its equilibrium position toward the positive direction. The speed of the motion of the parcel is in proportional to the degree of the instability.

Example 3 stable stratification (toss up)

Set the coefficients as follows:

0.0	0.4	-0.1	-0.075	-0.05	-0.025	0.0
Initial position	Initial velocity	dr/dz(1)	dr/dz(2)	dr/dz(3)	dr/dz(4)	dr/dz(5)

Status of stratification is the same as shown in Example 1. When the parcel is initially tossed up toward the positive direction, the result is the same as seen in Example 1, because the vibration period is only decided by the stratification. When initial velocities are the same, the amplitude depends on the status of stratification. The weaker the stratification is, the larger the amplitude is. In neutral density stratification (right side), the parcel moves away from equilibrium position with the initial velocity.

10.3   Appendix

Compare the results by assuming a positive displacement, a negative displacement, a toss up, and a toss down which are as shown in above examples. Although the motion of parcel in field of unstable stratification is unrealistic, it should be a meaningful subject for an experiment when we consider the fundamental of dynamics. There are series that only give a displacement to the parcel without initial velocity and series that make a positive displacement and then toss down. When we consider the motion of mass point in gravity potential field, it becomes meaningful for practice.

References

Shigeo Yoden, 2000: *Note of meteorology lecture I* (In Japanese)

Chapter 11

Thermal Convection

The thermal convection is driven by heterogeneous temperature field. When a fluid layer is heated from below and/or cooled from above, its thermal expansion yields a gravitationally unstable situation. Namely, the dense cool fluid tends to sink and the hot light fluid rises to generate a thermal convection. In this chapter, we will formulate the thermal convection of 2-dimensional non-compressible Newtonian fluid. The nature of the convection depends on two non-dimensional parameters, i.e., the Rayleigh number and the Prandtl number. We observe the generation and the growth of these convection currents in the numerical experiments.

11.1 Theoretical Background

11.1.1 Master equations

We suppose that a non-compressible Newtonian fluid of thickness d lies between horizontal rigid walls. The assumption of non-compressibility is called anelastic approximation. Independent variables x, z, t are horizontal and vertical (upward) coordinates and time, respectively, while dependent variables $\mathbf{u} = (u, v), p, \rho$ and T represent velocity, pressure, density and temperature. The temperature of the upper wall ($z = d$) and the lower wall ($z = 0$) are fixed at T_0 and at $T_0 + \Delta T (\Delta T > 0)$, respectively.

The thermal convection is described by the following three equations,

Navier-Stokes equation	$\rho \dfrac{D\mathbf{u}}{Dt} = -\nabla p + \eta \nabla^2 \mathbf{u} + \rho \mathbf{g},$	(11.1)
equation of continuity	$\rho \nabla \cdot \mathbf{u} = 0,$	(11.2)
equation of thermal advection and conduction	$\dfrac{DT}{Dt} = \kappa \nabla^2 T,$	(11.3)

where constants $\mathbf{g} = (0, -g), \eta$ and κ are the gravitational acceleration, the coefficient of viscosity and the thermal diffusivity. Equation (11.1) is the equation of motion for Newtonian fluid, while (11.2) corresponds to the conservation of mass for non-compressible fluid. The viscous heating and the internal heat generation are neglected.

For simplicity, we assume that density the ρ depends only on the temperature,

$$\rho = \rho_0 \{1 - \alpha(T - T_0)\}, \tag{11.4}$$

where constants ρ_0 and α are the density at temperature T_0 and the thermal expansion coefficient, respectively. Assuming that the change of density is small, we can neglect them except in the body force term of (11.1), $\rho \mathbf{g}$. That is so-called Boussinesq approximation, under which the above master

equations are expanded to be

$$\frac{\partial u}{\partial t} + u\frac{\partial u}{\partial x} + w\frac{\partial u}{\partial z} = -\frac{1}{\rho_0}\frac{\partial p}{\partial x} + \nu\nabla^2 u, \tag{11.5}$$

$$\frac{\partial w}{\partial t} + u\frac{\partial w}{\partial x} + w\frac{\partial w}{\partial z} = -\frac{1}{\rho_0}\frac{\partial p}{\partial z} + \nu\nabla^2 w - g\{1 - \alpha(T - T_0)\}, \tag{11.6}$$

$$\frac{\partial u}{\partial x} + \frac{\partial w}{\partial z} = 0, \tag{11.7}$$

$$\frac{\partial T}{\partial t} + u\frac{\partial T}{\partial x} + w\frac{\partial T}{\partial z} = \kappa\nabla^2 T, \tag{11.8}$$

where $\nu = \eta/\rho_0$ is the coefficient of kinematic viscosity.

11.1.2   Introduction of vorticity and stream function

The elimination of the pressure terms by $\frac{\partial}{\partial x}$ (11.6) $-\frac{\partial}{\partial z}$ (11.5) gives

$$\frac{\partial \zeta}{\partial t} + u\frac{\partial \zeta}{\partial x} + w\frac{\partial \zeta}{\partial z} = \nu\nabla^2\zeta + \alpha g\frac{\partial T}{\partial x},$$

where ζ is the y-component of the vorticity,

$$\zeta = \frac{\partial w}{\partial x} - \frac{\partial u}{\partial z}. \tag{11.9}$$

To satisfy (11.7), the stream function ψ is introduced,

$$u = -\frac{\partial \psi}{\partial z}, w = \frac{\partial \psi}{\partial x}. \tag{11.10}$$

The above two definitions show that the vorticity and the stream function are related by the Poisson's equation,

$$\zeta = \nabla^2\psi. \tag{11.11}$$

Using ζ and ψ, we can rewrite the master equations as

$$\frac{\partial \zeta}{\partial t} - \frac{\partial \psi}{\partial z}\frac{\partial \zeta}{\partial x} + \frac{\partial \psi}{\partial x}\frac{\partial \zeta}{\partial z} = \nu\nabla^2\zeta + \alpha g\frac{\partial T}{\partial x} \tag{11.12}$$

$$\frac{\partial T}{\partial t} - \frac{\partial \psi}{\partial z}\frac{\partial T}{\partial x} + \frac{\partial \psi}{\partial x}\frac{\partial T}{\partial z} = \kappa\nabla^2 T. \tag{11.13}$$

Consequently, we obtained the equations (11.11), (11.12) and (11.13) for unknown variables ψ, ζ and T. Note that (11.12) represents the generation and the advection of ζ caused by the *horizontal* temperature gradient ($\frac{\partial T}{\partial x}$). The generated vorticity yields the velocity field according to (11.11). Finally, that velocity field gives the new temperature field through (11.13). This circulation describes the generation and the growth of the thermal convection.

11.1.3   Non-dimensionalization

The master equations can be non-dimensionalized by normalizing length by d, time by the time scale of thermal diffusion, d^2/κ, and temperature by ΔT,

$$(x, z) = (d \cdot x^*, d \cdot z^*), \quad t = \frac{d^2}{\kappa}t^*, \quad \zeta = \frac{\kappa}{d^2}\zeta^*, \quad \psi = \kappa\psi^*, \quad T = \Delta T^*, \tag{11.14}$$

where the superscripts * represent non-dimensionalized variables. Equations (11.12) and (11.13) are rewritten as

$$\text{Pr}^{-1}\left(\frac{\partial \zeta^*}{\partial t^*} - \frac{\partial \psi^*}{\partial z^*}\frac{\partial \zeta^*}{\partial x^*} + \frac{\partial \psi^*}{\partial x^*}\frac{\partial \zeta^*}{\partial z^*}\right) = \nabla^2 \zeta^* + \text{Ra}\frac{\partial T^*}{\partial x^*}, \tag{11.15}$$

$$\frac{\partial T^*}{\partial t^*} - \frac{\partial \psi^*}{\partial z^*}\frac{\partial T^*}{\partial x^*} + \frac{\partial \psi^*}{\partial x^*}\frac{\partial T^*}{\partial z^*} = \nabla^2 T^*, \tag{11.16}$$

where two non-dimensional numbers Ra and Pr are the Rayleigh number and the Prandtl number, respectively. They are defined as

$$\text{Ra} = \frac{\alpha g d^3 \Delta T}{\kappa \nu}, \quad \text{Pr} = \frac{\nu}{\kappa}. \tag{11.17}$$

Ra is a ratio between the time scale of the thermal conduction and that of the thermal advection. A large Ra means that the advection is more efficient than the conduction for the heat transport, and causes the thermal convection. According to the linear stability theory, the convection occurs when Ra exceeds the critical value Ra_c which is order of 10^3. If the Ra is substantially large, the convection shifts to turbulent flow.

Meanwhile, Pr is a ratio between the thermal diffusivity and the diffusivity of momentum, i.e., the kinematic viscosity. In such a case of the earth's mantle convection, a large value of ν makes the inertia terms in (11.15) negligible.

11.2 Exercises

11.2.1 Boundary and initial conditions

Equations (11.11), (11.15) and (11.16) are solved to determine velocity, vorticity and temperature fields under the following boundary and initial conditions. On the lower and upper walls ($z = 0, d$), the temperature is fixed,

$$T = \begin{cases} T_0 + \Delta T & (z = 0) \\ T_0. & (z = d) \end{cases} \tag{11.18}$$

The computational domain is rectangular with height (depth) d and width $l = 2d$. On all the walls, the fluid slips freely with no viscous stress (stress-free condition),

$$w = 0, \quad \frac{\partial u}{\partial z} + \frac{\partial w}{\partial x} = 0. \quad (x = 0, 2d, \quad z = 0, d)$$

The above mechanical conditions are equivalent to

$$\psi = 0, \quad \zeta = \frac{\partial^2 \psi}{\partial z^2} = 0. \quad (x = 0, 2d, \quad z = 0, d) \tag{11.19}$$

The initial conditions are given as

$$\zeta = 0, \quad T = T_0, \quad \psi = 0. \quad (t = 0) \tag{11.20}$$

Since the convectional current cannot occur without any horizontal temperature gradient as we have seen in (11.12), a small perturbation in temperature is given at the center of the domain,

$$T(x = d, z = \frac{d}{2}) = T_0 + 0.1\Delta T. \tag{11.21}$$

In the calculations, the time step Δt must satisfy the following condition to obtain stable solution,

$$\Delta t < \min\left(\frac{1}{\nu(k_{\max}^2 + l_{\max}^2)}, \frac{1}{\kappa(k_{\max}^2 + l_{\max}^2)}\right), \tag{11.22}$$

where $k_{\max} = \pi/\Delta x, l_{\max} = \pi/\Delta z$, and where Δx and Δz are the spatial grid sizes of the horizotal and vertical directions, respectively.
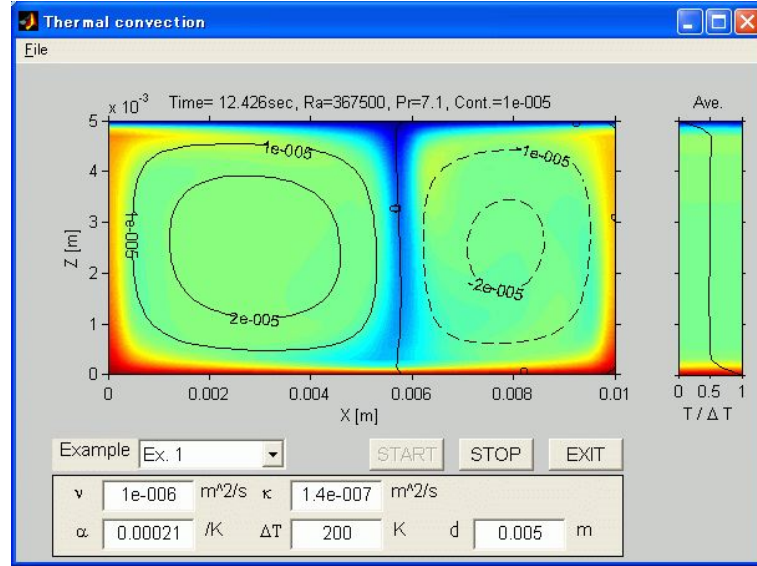
Figure 11.1: Result of Example 1.

11.2.2   Standard experiment

For instance, the water in a pot heated from bottom has such parameters as

$$\nu = 10^{-6} \text{ m}^2/\text{s}, \qquad g = 9.8 \text{ m/s}^2, \quad \kappa = 1.4 \times 10^{-7} \text{ m}^2/\text{s},$$
$$\alpha = 2.1 \times 10^{-4} \text{ /K}, \quad \Delta T = 200 \text{ K}, \quad d = 0.005 \text{ m},$$

for which the non-dimensional numbers are Ra= 1.5×10^9 and Pr= 7.1. Since Ra clearly exceeds Ra$_c$, the thermal convection occurs in the pot.

11.3   Appendix

In the program of the thermal convection, the main contour plot shows the stream function ψ. According to the definition (11.10), the convection currents occur along the contour lines clockwise around the domain of higher ψ, and counterclockwise around that of lower ψ.

The plot in the right shows the temperature averaged in horizontal (x) direction. When the thermal transport is performed mainly by the thermal conduction, the x-averaged temperature linearly increases with depth. Once the convection takes place, the most part of the fluid layer has a constant x-averaged temperature, although there exist the vertical movements of hot and cold plumes. Meanwhile, in the top and the bottom of the fluid layer, the x-averaged temperature drastically varies to form the thermal boundary layers, of which thicknesses depend on the Prandtl number, Pr.

Change the parameters, Ra and Pr, and observe the development of the velocity and the temperature fields.

Chapter 12

Chaos and Predictability

In this chapter we study the structure of the strange attractor by use of the well-known chaos model of Lorenz(1963), and perform some basic experiments concerning the predictability.

12.1   Theoretical Background

We assume that $X = X(t)$ represents the intensity of the convective motion, $Y = Y(t)$ represents the temperature difference between the ascending and the descending current, and $Z = Z(t)$ represents the deviation of the vertical temperature profile from linearity. By approximating extremely the partial differential equations of the heat convection, Edward Lorenz derived the following set of the simple three ordinary differential equations,

$$\frac{dX}{dt} = -\sigma X + \sigma Y \tag{12.1}$$

$$\frac{dY}{dt} = -XZ + \gamma X - Y \tag{12.2}$$

$$\frac{dY}{dt} = XY - bZ \tag{12.3}$$

where σ, γ, and b denote the Prandtl number, the Rayleigh number, and the spatical periodicity of the convection, respectively.

Lorenz discovered *chaos* by performing time-integration of the above equations numerically in the old days when the computer had not developed enough. He expressed chaos as 'an irregular motion under determinism' in his monumental paper (Lorenz, 1963).

Lorentz (1963) described the numerical solution at $\sigma = 10, b = 8/3, \gamma = 28$. Assuming σ as 10 and b as 8/3, we study the dependence of the stability of the solution on γ. For $0 \leq \gamma \leq 1$, the steady state is only the heat conduction (Berge et al., 1984),

$$X = Y = Z = 0. \tag{12.4}$$

For γ slightly larger than 1, the solution of the heat conduction becomes unstable, while other two solutions arise

$$X = Y = \pm[b(\gamma - 1)]^{1/2}, \quad Z = \gamma - 1. \tag{12.5}$$

They represent the steady convection. Although these two solutions are linearly stable for $1 \leq \gamma \leq 24.74$, they become unstable for $\gamma = 24.74$, and for $\gamma > 24.74$ only nonperiodic solutions exist.

In more detail, for $24.06 < \gamma < 24.74$ the three *attractors* (a region attracting a trajectory in *phase space*) coexist so that *hysteresis* is observed. One of them is a *strange atrractor*, and the others are the steaty heat convection already mentioned. That strange attractor which appears for $\gamma < 24.74$ is called as a *non-standard* strange attractor, and chaos exists quasi-stable (*meta stable chaos*) for $\gamma > 13.926$. For $24.74 < \gamma < 30.4$, only the strange attractor exists stable. It may be the reason why many numerical studies have done at $\gamma = 28$.
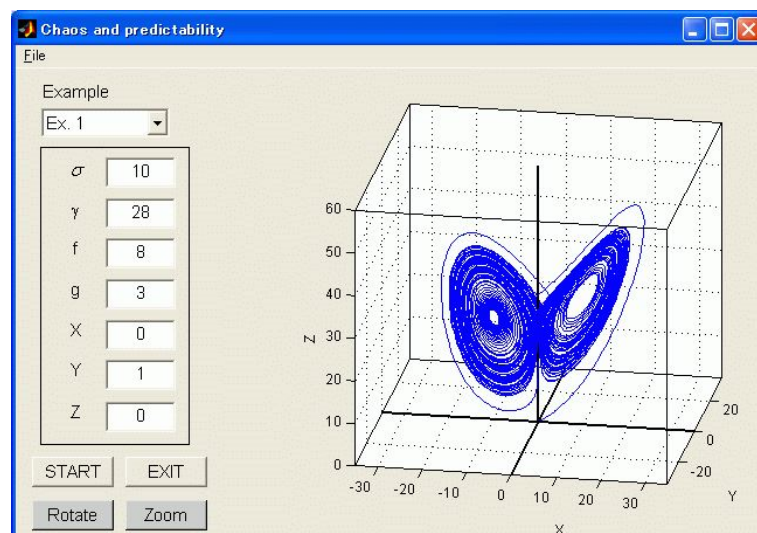
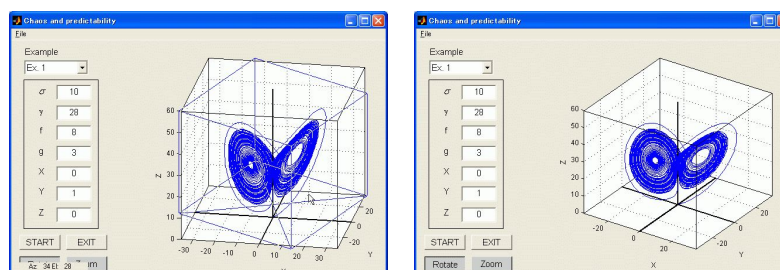Figure 12.1: Result of "C12-1" using parameters of Example 1.

Figure 12.2: Samples rotating the result of "C12-1" shown in Figure 12.1.

12.2   Exercises

Perform exercises about Lorenz Chaos by using the programs "C12-1", "C12-2", and "C12-3". By dragging the graphic window as shown in Figure 12.2, we can rotate the result of both "C12-1" and "C12-2" and observe from various view angles. These programs use the Runge-Kutta-Gill method for numerical integration.

12.2.1   Exercise 1 - the Lorenz attractor

Set the parameters as the same as the Lorenz's experiment ($\sigma = 10, b = 8/3, \gamma = 28$, the initial condition $(X, Y, Z) = (0, 1, 0)$), and view a three-dimensional image of a strange attractor from various angles to comprehend its characteristic structure. Note that the parameter b is expressed as `f/g` in the program.

Example 1 The standard experiment.

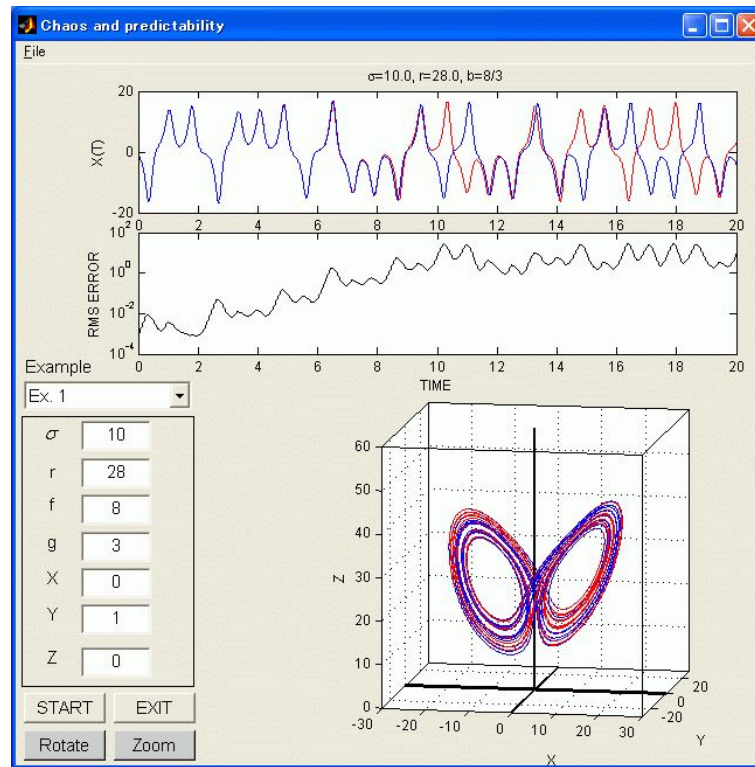| 10.0	28.0	8.0	3.0	0.0	1.0	0.0
σ	γ	f	g	X	Y	Z

Figure 12.3: Result of "C12-2" using parameters of Example 1.

12.2.2 Exercise 2 - various strange attractors

In this section, display various strange attractors by changing the parameters ($\sigma, b, \gamma, X, Y, Z$), and perform some applied experiments to have a profound understanding of chaos itself. The programs used here are `lore3` and `lore4`.

- "C12-2" shows sharp dependence of chaos on the initial state. Lorenz(1997) explained *sharp dependence on the initial state* as follows. Two states subjected to determinism will keep identical if the current states are perfectly identical. On the other hand, if there is a slight difference between the current states, the difference will grow with the course of time, so that the two states will be quite different. We may say that phenomena with this nature, *sharp dependence on the initial state*, are *chaotic*.

- "C12-3" displays a *Lorenz plot*. The abscissa is Z_n, the value of the nth maximum of a variable Z, while the ordinate is Z_{n+1}, the value of the following maximum. Each point represents a mapping from Z_n to Z_{n+1}. Lorenz idealized this Lorenz plot as a two-to-one correspondence, and examine its property to argue the nature of chaos.

After running both "C12-2" and "C12-3" using the previous parameters, change the constants σ, γ, and b to examine the parameter dependence of solutions of the system. Note that $\sigma = 10.0$, where σ is the Prandtl number, corresponds to a value of water. If you want to perform the experiments concerning a convection in the air, change the value of σ as 1.0.

Example 2 Set the parameters as follows,

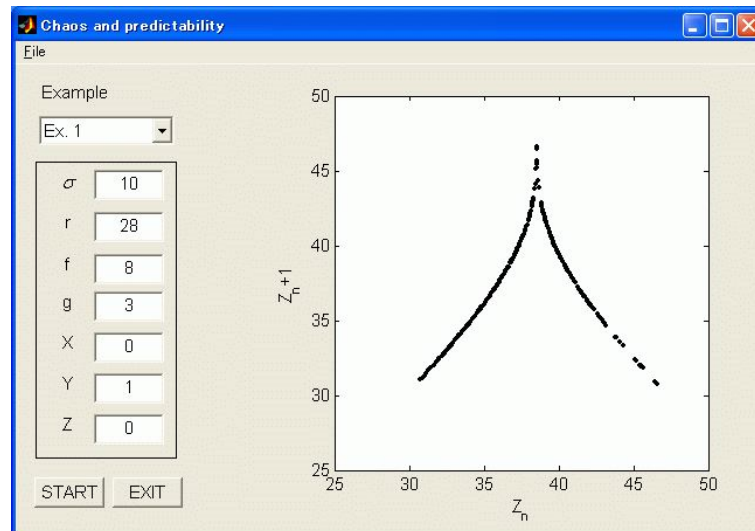| 10.0	28.0	8.0	3.0	30.0	30.0	30.0
σ	γ	f	g	X	Y	Z

Figure 12.4: Result of "C12-3" using parameters of Example 1.

Perform the programs with another set of parameters in (X, Y, Z) which corresponds to the initial state. Consider the reason why either a steady state or a strange attractor appears dependent on the initial state even we assume the same value of σ.

12.3   Appendix

Lorenz (1997,p10) said as follows.

> 'Under any system sharply dependent on the initial state, it is impossible to predict the sufficiently distant future even at a mediocre level, unless perfectly accurate observations are available.'

In weather forecasting, *daily forecast* is one of the problems due to the sensitivity on the initial state; this sensitivity is arising from a chaotic nature of the atmosphere. In medium-range (1 to 2 weeks) forecasting at mid-latitudes, we often find that a predicted state changes significantly at every update of the initial state, and a next prediction is not always better than a previous one (Tsuyuki 1999). In recent years, this is one of the serious problems for improving the accuracy of medium-range forecasting. It will be interesting to cite some methods adopted today to handle this problem and consider their merits.

Reference

E. N. Lorenz, 1963 : Deterministic Nonperiodic flow, *J. Asmos. Sci.*, **20**, 130-141

P. Berge, Y.Pomeau, C.Vidal, 1984 : L'ordre dans le chaos - vers une approche deterministe de la turbulence

E. N. Lorenz, 1996 : The Essence of Chaos (The Jessie and John Danz Lecture Series), *Univ. of Washington Press*

Tsuyuki, 1999 : Data assimilation and sensitivity on the initial state, *Tenki*, **46-3**, 179-184 (in Japanese)

List of Contributors

Shigeo Yoden
Meteorology and Atmospheric Physics,
Department of Geophysics,
Graduate School of Science, Kyoto University

Satoshi Sakai
Department of Interdisciplinary Environment,
Graduate School of Human and Environmental
Studies, Kyoto University

Toshihiko Iyemori
Solar-Planetary Electromagnetism Labratory,
Department of Geophysics,
Graduate School of Science, Kyoto University

Yoshiharu Omura
Research Institute for Sustainable
Humanosphere, Kyoto University

and KAGI21 K2

Collaborators

Yuto Katoh
Research Institute for Sustainable
Humanosphere, Kyoto University

Shin'ya Nakano
Solar-Planetary Electromagnetism Labratory,
Department of Geophysics,
Graduate School of Science, Kyoto University

Koichi Shin
Research Institute for Sustainable
Humanosphere, Kyoto University

Research Assistants

Atsushi Hamada
Physical Climate, Department of Geophysics,
Graduate School of Science, Kyoto University

Desheng Han
Solar-Planetary Electromagnetism Labratory,
Department of Geophysics,
Graduate School of Science, Kyoto University

Junko Nakata
Physical Climate, Department of Geophysics,
Graduate School of Science, Kyoto University

Shigenori Otsuka
Meteorology and Atmospheric Physics,
Department of Geophysics,
Graduate School of Science, Kyoto University

Kei Sakamoto
Physical Oceanography,
Department of Geophysics,
Graduate School of Science, Kyoto University

Katsushi Sato
Historical Geoscience of the Biosphere,
Department of Geology and Mineralogy,
Graduate School of Science, Kyoto University

Hisahiro Takashima
Research Institute for Sustainable
Humanosphere, Kyoto University

Satoru Yokoi
Physical Climate, Department of Geophysics,
Graduate School of Science, Kyoto University

Daiki Yoshida
Solar-Planetary Electromagnetism Labratory,
Department of Geophysics,
Graduate School of Science, Kyoto University